Icarus 212 (2011) 682–696

Contents lists available at ScienceDirect

Icarus

journal homepage: www.elsevier.com/locate/icarus

IRTF spectra for 17 asteroids from the C and X complexes: A discussion of continuum slopes and their relationships to C chondrites and phyllosilicates

Daniel R. Ostrowski [a], Claud H.S. Lacy [a,b], Katherine M. Gietzen [a], Derek W.G. Sears [a,c,*]

[a] Arkansas Center for Space and Planetary Sciences, University of Arkansas, Fayetteville, AR 72701, United States
[b] Department of Physics, University of Arkansas, Fayetteville, AR 72701, United States
[c] Department of Chemistry and Biochemistry, University of Arkansas, Fayetteville, AR 72701, United States

ARTICLE INFO

Article history:
Received 23 April 2009
Revised 20 January 2011
Accepted 25 January 2011
Available online 1 February 2011

Keywords:
Asteroids, composition
Spectroscopy
Meteorites
Mineralogy

ABSTRACT

In order to gain further insight into their surface compositions and relationships with meteorites, we have obtained spectra for 17 C and X complex asteroids using NASA's Infrared Telescope Facility and SpeX infrared spectrometer. We augment these spectra with data in the visible region taken from the on-line databases. Only one of the 17 asteroids showed the three features usually associated with water, the UV slope, a 0.7 μm feature and a 3 μm feature, while five show no evidence for water and 11 had one or two of these features. According to DeMeo et al. (2009), whose asteroid classification scheme we use here, 88% of the variance in asteroid spectra is explained by continuum slope so that asteroids can also be characterized by the slopes of their continua. We thus plot the slope of the continuum between 1.8 and 2.5 μm against slope between 1.0 and 1.75 μm, the break at ~1.8 μm chosen since phyllosilicates show numerous water-related features beyond this wavelength. On such plots, the C complex fields match those of phyllosilicates kaolinite and montmorillonite that have been heated to about 700 °C, while the X complex fields match the fields for phyllosilicates montmorillonite and serpentine that have been similarly heated. We thus suggest that the surface of the C complex asteroids consist of decomposition products of kaolinite or montmorillonite while for the X complex we suggest that surfaces consist of decomposition products of montmorillonite or serpentine. On the basis of overlapping in fields on the continuum plots we suggest that the CI chondrites are linked with the Cgh asteroids, individual CV and CR chondrites are linked with Xc asteroids, a CK chondrite is linked with the Ch or Cgh asteroids, a number of unusual CI/CM meteorites are linked with C asteroids, and the CM chondrites are linked with the Xk asteroids. The associations are in reasonable agreement with chondrite mineralogy and albedo data.

1. Introduction

As part of a project to characterize the surface of asteroids and the asteroid–meteorite linkage, especially for potential mission targets (Sears et al., 2004), we have measured near-IR spectra for near-Earth and main-belt asteroids using NASA's Infrared Telescope Facility in Hawaii and the SpeX spectrometer with a range of 0.8–2.5 μm. Here we report data for 17 C and X complex asteroids. Elsewhere we report data for S and V asteroids (Gietzen et al., submitted for publication).

The C, X and related classes were originally defined by Bus and Binzel (2002) using visible spectra, as a development of the Tholen (1989) scheme. Their approach is based on a Principal Component Analysis that identified absorption in the UV, absorption around 0.9 μm, and the continuum slope as the most significant factors in characterizing asteroid spectra. In addition, a 0.7 μm feature that has been reported in about half of the C complex asteroids, and correlates with a much stronger water-related absorption feature at 3 μm, is also used in taxonomy (Lebofsky, 1978, 1980; Feierberg et al., 1985a; Vilas and Gaffey, 1989; Vilas, 1994; Jones et al., 1990; Fornasier et al., 1999; see Rivkin et al. (2002) for a review). DeMeo et al. (2009) recently folded near infrared data into the taxonomy, with a few modifications, and their scheme will be used throughout this paper.

Because of their low albedos, generally weak features (compared, for example, with the S asteroids), and occasional evidence for water-related features, the C asteroids have frequently been linked to carbonaceous chondrites, specifically the CI and CM chondrites (Vilas and Gaffey, 1989; Vilas et al., 1993; Vilas, 1994). The CI chondrites were originally linked to C asteroids by Gaffey and McCord (1978), while the CM chondrites have been linked with the Fortuna Ch asteroid by Burbine (1998). More recently, Carvano et al. (2003) linked the CM chondrites to any asteroid that had a 0.7 μm band. The CI and CM chondrites are the meteorites that

* Corresponding author at: Arkansas Center for Space and Planetary Sciences, University of Arkansas, Fayetteville, AR 72701, United States.
E-mail address: dsears@uark.edu (D.W.G. Sears).

0019-1035/$ - see front matter © 2011 Elsevier Inc. All rights reserved.
doi:10.1016/j.icarus.2011.01.032

are closest to the solar photosphere in composition and they contain abundant water, up to 10 vol.% for the CM chondrites and up to 20 vol.% for the CI chondrites (Wiik, 1969; Jarosewich, 1990).

In addition to the water-rich CI and CM chondrites, other C chondrite classes include the anhydrous CO and CV chondrites, the anhydrous metal-rich CH chondrites, and several others. The CO and CV chondrites have been linked to K asteroids by Bell (1988). The small CR class was linked to C asteroids by Hiroi et al. (1996) and equally small CK chondrite class and was linked to C asteroids by Gaffey and McCord (1978). The CH chondrites have been linked to C or M asteroids by Burbine et al. (2002). Carvano et al. (2003) linked the CK chondrites to B asteroids (that are included in the C asteroid complex).

It is very difficult to characterize the mineralogy of CI and CM chondrites since they seem to consist largely of amorphous silicate phases intermixed with microscopic sulfide and metal grains. This mixed phase was once called "PCP" (for "poorly characterized phase"), but is now termed tochilonite (Barber et al., 1983; Mackinnon and Zolensky, 1984; Tomeoka and Buseck, 1985; Brearley, 2006). It is sometimes possible to find fine-scale regions of a recognizable phyllosilicate phase, such as serpentine and chlorite (Brearley, 2006), and indirect inferences based on bulk chemistry have been used to characterize the phyllosilicate phase in meteorites (McSween and Richardson, 1977). Vilas and Gaffey (1989) suggested serpentine and chlorite as possible phyllosilicates on the surface of low albedo asteroids. In their review of spectroscopic information on the nature of the surface of C and X complex asteroids, Rivkin et al. (2002) inferred the presence of hydrated phases including phyllosilicates. Rivkin (1997) and Rivkin et al. (2006) suggested that the surface of C asteroid Ceres contained an ammoniated smectite, such as ammoniated cronstedtite.

The surface of an asteroid is heavily altered as a result of exposure to the space environment. Radiation damage by solar wind and solar energetic particles, micrometeorite bombardment, and major meteorite impacts will have affected the surface. The surfaces of all asteroids visited by spacecraft to date are heavily impacted, and are thus covered with unconsolidated regolith (e.g. Sullivan et al., 2002). Thus Hiroi and Zolensky (1999) performed heat treatments on terrestrial phyllosilicates, three members of the serpentine group (antigorite, lizardite, clinochrysotile), chlorite, and saponite. They considered albedo, UV absorption, the 0.7 μm band, and the 3.0 μm band and they compared their heated phyllosilicate spectra with those of the asteroids. These authors concluded that the best fit for the phyllosilicate on the asteroid surfaces was saponite, but were concerned that this mineral had not been observed in meteorites.

Ostrowski et al. (2010) recently reported data for a series of heated phyllosilicates that covered and extended the range of samples examined by Hiroi and his colleagues and took the experiments to higher temperatures where more complete destruction of the phyllosilicates occurs. In this paper we report results of a detailed comparison of spectra for asteroids, meteorites, and heated phyllosilicates and discuss implications for asteroid–meteorite linkage and asteroid surface composition. Preliminary reports have been made at various conferences (Ostrowski et al., 2008a,b, 2009a,b; Sears et al., 2008a,b), but the data and conclusions reported here supersede them.

2. Methods

Our spectra were obtained using the NASA's Infrared Telescope Facility on Mauna Kea, Hawaii, and the SpeX infrared spectrometer in low-resolution prism mode over 0.8–2.5 μm (Rayner et al. 2003), between 2004 August 6 and 2008 April 18 (Table 1). We were able to obtain useful spectra for asteroids as faint as magnitude 17.5. The raw data were reduced by using IRAF and IDL software which eliminated instrumental and atmospheric artifacts, normalized to solar analogue spectra, and produced wavelength-calibrated spectra with a resolution of 5 nm.

Much of our discussion below will relate to the slope of the spectral continuum. There is much precedence for using slope in studies of asteroid spectra. As mentioned above, DeMeo et al. (2009) found that 88% of the variance in asteroid spectra is

Table 1
Observational details for the present asteroids*.

Asteroid number	Asteroid name	UT date	Exposure (s)	Air mass	Visual magnitude	Sky conditions	Analog stars	Solar elongation (degrees)
24	Themis	4/18/2008	300(10)	1.019	12.3	c, m	5, 6, 8	−92.9
34	Circe	4/14/2005	720(6)	1.222	12.4		8, 9, 11	144.7
45	Eugenia	4/14/2005	320(4)	1.185	11.3		8, 9, 11	141
51	Nemausa	10/14/2005	200(4)	1.071	10.8		2, 3, 13	−166.7
52	Europa	5/30/2006	160(4)	1.106	11.3		7, 8, 9, 11	−148.3
77	Frigga	1/22/2008	720(6)	1.113	12.8	m	2, 3, 5, 7	133.5
87	Sylvia	10/14/2005	400(8)	1.004	12.1		2, 3, 13	139.4
88	Thisbe	10/14/2005	240(8)	1.006	11.3		2, 3, 13	145.5
93	Minerva	10/14/2005	400(8)	1.025	12.8		2, 3, 13	123.2
129	Antigone	4/14/2005	240(8)	1.055	10.2		8, 9, 11	148.3
140	Siwa	12/29/2006	480(4)	1.004	13.4		3, 4, 5	164.2
181	Eucharis	5/30/2006	480(4)	1.007	13.3		7, 8, 9, 11	−128.4
191	Kolga	4/14/2005	960(8)	1.135	13.9		8, 9, 11	127.7
213	Lilaea	12/29/2006	160(4)	1	13.3		3, 4, 5	−171.6
3691	Bede	1/22/2008	960(8)	1.033	16.9	m	2, 3, 5, 7	111.3
7753	1988 XB	12/3/2004	3600(30)	1.021	15.1		1, 2, 5, 6	131.2
153591	2001 SN263	1/22/2008	1560(13)	1.165	14.2	m	2, 3, 5, 7	−122.9
153591(b)	2001 SN263	4/18/2008	1920(16)	1.408	15.6	c, m	5, 6, 8	−148.6

Exposure: The total exposure time, in seconds, followed by the number of CCD images (in parentheses) that were combined to produce the total exposure time.
Air mass: Mean air mass of the observations, calculated from the air mass values recorded at the start of each exposure.
Visual magnitude: Calculated visual (V-band) magnitude of the asteroid at the time of the observation.
Sky conditions: Sky conditions at the time of the observation, where *c* is for cloudy, roughly defined as the presence of clouds that led to erratic variations (greater than 5%) in the observed flux of either the solar-analog star or the asteroid, *h* is for a relative humidity greater than 70%, and *m* is for moonlight, where the lunar illumination is greater than 50%, and the Moon's altitude above the horizon is greater than 20°.
Analog stars: The solar-analog star used in the calibration of the asteroid spectrum. 1: Land 92–276; 2: Land 93–101; 3: Hyades 64; 4: Land 97–249; 5: Land 98–978; 6: Land 102–1081; 7: Land 103–487; 8: 105–56; 9: 107–684; 10: Land 107–998; 11: Land 110–361; 12: Land 112–1333; 13: Land 113–276; 14: Land 115–271.
Solar elongation: The angle between the Sun and the asteroid at the time of observation.
* Digital files of the spectra can be found at the following web site (http://www.uark.edu/misc/clacy/SpeX_site/index.htm).

explained by continuum slope and slope features in the qualitative descriptions of most C and X classes in their paper. Hiroi et al. (1993, 1996) performed spectral matching between heated phyllosilicates, C chondrites, and C asteroids that are generally featureless, so that his method amounts to slope comparison. A recent paper by Clark et al. (2010) also emphasizes continuum slope of B asteroids in an effort to find meteorite analogs.

We will quantify the overall shape of the spectra in the near-IR region by dividing the spectra into two more-or-less equal halves (1.0–1.75 μm and 1.8–2.5 μm), as shown in Fig. 1. We make the break at 1.8 μm because it is beyond this wavelength that a number of large water features are present in phyllosilicates (e.g. Ostrowski et al., 2010). A plot of the longer wavelength interval against the shorter wavelength interval we call the "continuum plot" (Ostrowski et al., 2010).

Many experimental factors have the potential to affect continuum slope, such as placement on the slit, differential refraction, diffraction, and atmospheric variations. The asteroids and solar analogue stars in the present study were within 15 degrees of the meridian so as to minimize the effects of differential refraction. Dispersion was normal to the slit so when the target was kept near the meridian the atmospheric dispersion was along the slit and the entire signal along the slit was included in the data reduction. Automatic tracking and guidance kept the asteroid centered on the slit so the diffracted image overfilled it, manual corrections being used when necessary, and the infrared slit-viewing camera continuously monitored the object's position on the 0.8 arcsec slit. We corrected for atmospheric variations using the methods of Vacca et al. (2003) for the specific zenith distance of the object. The clustering of slope data and resolution of various groups of objects (C and X asteroids and CM chondrites, for instance), and the reproducibility of the slope data when determined by different research groups, are indications that these continuum measurements are not dominated by these sources of scatter.

3. Results

The spectra for the asteroids we observed are shown in Fig. 2a. Digital files of these spectra are available at our web site (http://www.uark.edu/misc/clacy/SpeX_site/index.htm). The spectra of Asteroid 7753 and the two observations of Asteroid 153591 show an increase in intensity at the long wavelengths due to the

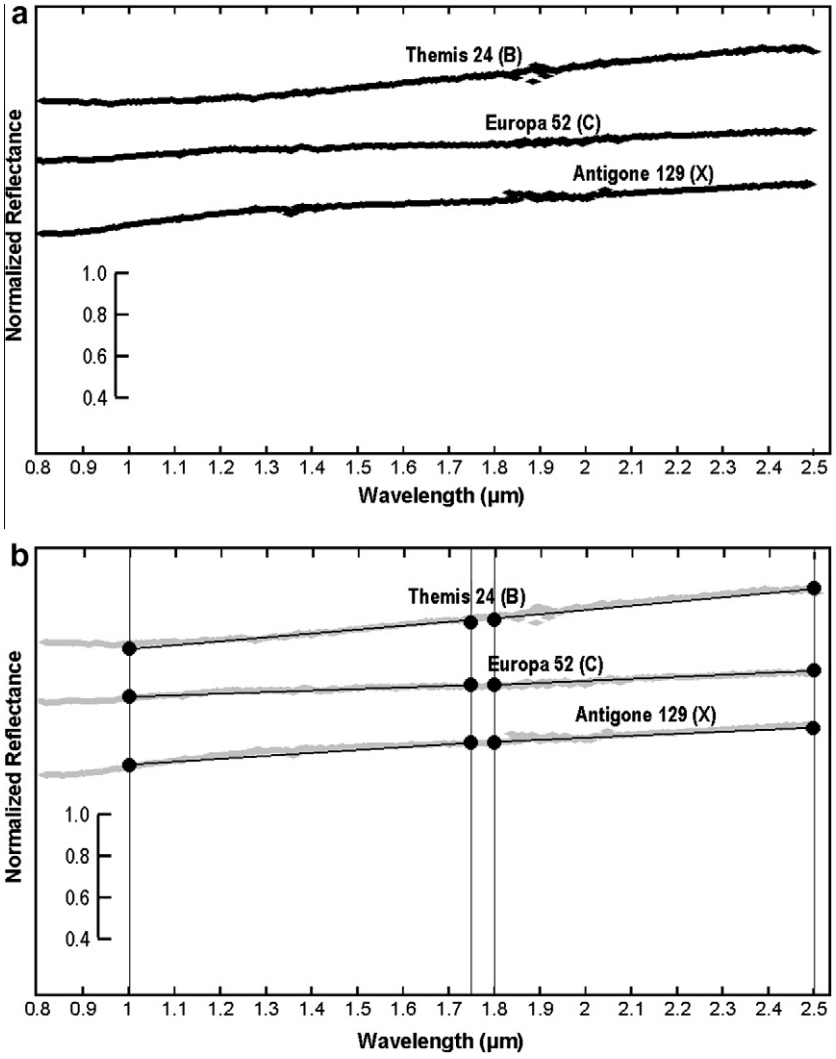

Fig. 1. (a) Representative spectra for three asteroids; 153591 2001 SN263 (B), 52 Europa (C), and 129 Antigone (Xk), displaced on the vertical scale for clarity. Note the lack of major absorption features in the spectra. (b) Explanation for the manner in which we quantify the main features of these spectra using "continuum slopes" over the two wavelength intervals, 1.0–1.75 μm and 1.8–2.5 μm. The break at 1.8 μm was selected because of a frequent change in slope observed for terrestrial phyllosilicates at the wavelength due to the large number of water-related bands possible in the longer wavelength interval. For the purposes of determining slopes, the spectra are normalized to 0.875 μm.

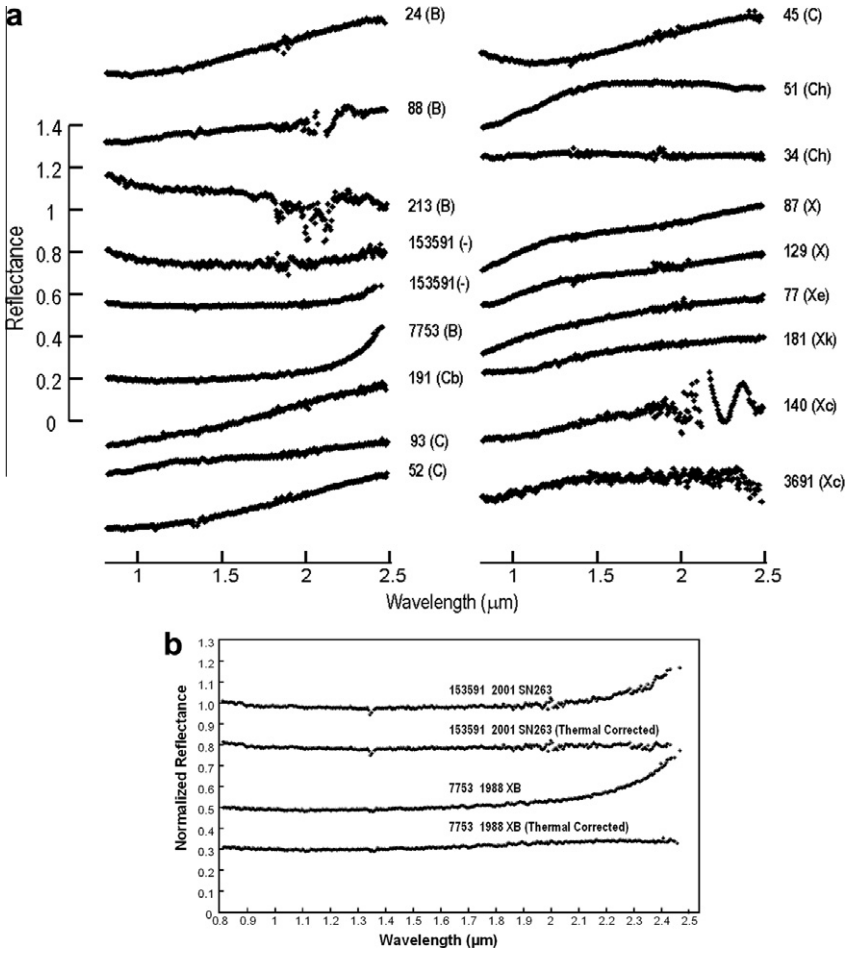

Fig. 2. (a) Raw spectra of asteroids from the B, C and X complexes observed in this study, displaced on a vertical scale for clarity. The quoted classes (in parentheses) are from the system of DeMeo et al. (2009). Most of the observed asteroids are relatively flat and featureless and the slope of their continua seems the major discriminator between them and is the basis for comparison in the present paper. (The small feature at ~1.35 μm and the anomalous features at longer wavelengths are due to terrestrial atmospheric water.) (b) Asteroids 153591 and 7753 show evidence for thermal emission at long wavelengths, which was removed prior to analysis using the method of Rivkin et al. (2005).

presence of thermal emission. This effect has been removed from the data using the method of Rivkin et al. (2005) and the results are shown in Fig. 2b. This method includes the effects of albedo and "beaming" along with the phase angle of observation.

In general the near-IR spectra we obtained are flat and featureless. Most show positive continuum slopes except for 213 Lilea where it is negative. A few show a notable change in slope, for example 51 Nemausa has an inflection at ~1.5 μm, and 87 Sylvia and 129 Antigone have slope changes at ~1.25 μm. The data and the continuum plot for the present asteroids appear in Table 2, where the uncertainties are calculated by determining the upper most slope and the lower most slope the scatter in the spectra will allow, and the values are plotted in Fig. 3. The distinction between C and X asteroids is readily apparent in Fig. 3. The two diagonal lines are naked-eye estimates of the trends for the C and X complex asteroids. In fact, this plot is a quantitative and visual summary of the class designations in Table 3 and the descriptions in Table 4, where the asteroid classes are defined and where C complex asteroids are said to have a "slightly positive" slope and the X complex asteroids have a "slight to moderate" slope. The anomalous asteroid, 51 Nemausa (Cgh), is anomalous for its positive slope at the shorter wavelengths (see Fig. 2).

The only absorption features we observed in our spectra are weak bands at 1.35 μm, which appear in 12 of our 18 spectra which are due to telluric water since several display spectral reversals (e.g. 88 Thisbe, 34 Chicago, 52 Europa). Gaffey (2003) discussed this issue. The features seen in the long wavelength region for Asteroids 88 (Cb), 213 (B) and 140 (Xc) are also telluric

Table 2
Continuum slope and albedo data for the present asteroids.

Asteroid	Short λ slope	Long λ slope	Albedo[a]
24 Themis	0.175 ± 0.014	0.197 ± 0.017	0.067
34 Circe	0.009 ± 0.001	0.003 ± 0.001	0.0541
45 Eugenia	0.127 ± 0.004	0.169 ± 0.001	0.0398
51 Nemausa	0.235 ± 0.004	−0.036 ± 0.007	0.0928
52 Europa	0.135 ± 0.002	0.224 ± 0.006	0.0578
77 Frigga	0.213 ± 0.009	0.091 ± 0.005	0.144
87 Sylvia	0.189 ± 0.002	0.176 ± 0.004	0.0435
88 Thisbe	0.092 ± 0.001	0.113 ± 0.001	0.0671
93 Minerva	0.080 ± 0.002	0.106 ± 0.006	0.0733
129 Antigone	0.167 ± 0.003	0.139 ± 0.005	0.164
140 Siwa	0.164 ± 0.003	−0.014 ± 0.007	0.0676
181 Eucharis	0.156 ± 0.003	0.073 ± 0.001	0.1135
191 Kolga	0.165 ± 0.008	0.204 ± 0.005	0.0408
213 Lilaea	−0.059 ± 0.004	−0.061 ± 0.006	0.0897
3691 Bede	0.114 ± 0.011	−0.089 ± 0.012	
7753 1988 XB[b]	0.025 ± 0.001	0.034 ± 0.001	
153591 2001 SN263	−0.002 ± 0.002	0.020 ± 0.006	
153591 2001 SN263[b,c]	−0.033 ± 0.005	0.064 ± 0.004	

[a] Albedo data from Chamberlin and Yeomans (2010).
[b] Corrected for thermal radiation.
[c] Duplicate observation.

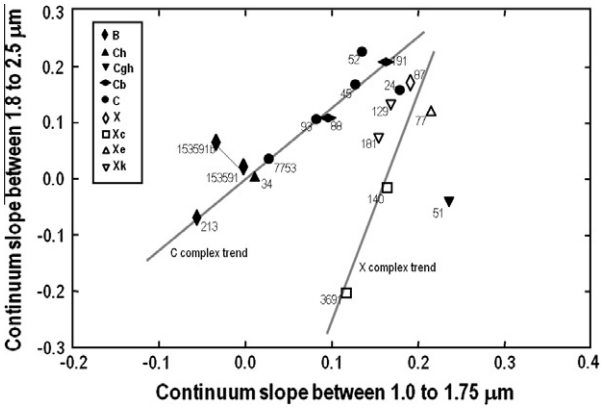

Fig. 3. A continuum plot for C and X complex asteroids observed in the present study. Two possible trend lines are indicated, one passing through the C asteroids and one passing through the X asteroids. There is one anomalous Cgh asteroid, 51 Nemausa, whose spectrum has an unusual change in slope at ~1.5 μm (see Fig. 2).

Table 3
Classification of the asteroids observed in the present study.

Asteroid		Taxonomy		
Number	Name	Tholen (1989)	Bus and Binzel (2002)	DeMeo et al. (2009)
24	Themis	C	B	C
34	Circe	C	Ch	Ch
45	Eugenia	FC	C	C[a]
51	Nemausa	CU	Ch	Cgh
52	Europa	CF	C	C
77	Frigga	MU	Xe	Xe
87	Sylvia	P	X	X
88	Thisbe	CF	B	Cb[a]
93	Minerva	CU	C	C
129	Antigone	M	X	Xk[a]
140	Siwa	P	Xc	Xc[a]
181	Eucharis	S	Xk	Xk
191	Kolga	XC	Cb	Cb
213	Lilaea	F	B	B[a]
3691	Bede		Xc	Xc[a]
7753	1988 XB		B	C[a]
153591	2001 SN263			B[a]

[a] Classifications determined by applying the DeMeo et al. (2009) software (available at http://www.smass.mit.edu/cgi-bin/busdemeoclass-cgi) to the present spectra.

Table 4
Description of the classes with respect to slope and water-related features for the present asteroids (after DeMeo et al. (2009)).

	Slope	Water-related features[a]		
		UV	0.7 μm	Other
B	Linear, negative, bump 0.6 μm, dip 1–2 μm	NA	NA	NA
C	Linear, flat, bump 0.6, positive >1.3 μm	NA	NA	>1 μm?
Ch	Slight positive >1.1 μm	UV drop off	Shallow	NA
Cgh	Slight positive >1 μm	Pronounced UV drop off	Broad, shallow	NA
Cb	Linear, slight positive >1.1 μm	NA	NA	NA
X	Linear, medium to high	NA	NA	NA
Xc	Low to medium, slightly curved concave downward	NA	NA	NA
Xe	Low to medium, like Xc	NA	NA	<0.55 μm
Xk	Like Xc	NA	NA	0.8–1.0 μm, weak

[a] NA, not applicable, means that the feature is absent or not relevant to the definition of the class.

water features that have not been completely removed by our correction procedures. These features do not seem to have affected their continuum slopes, judging by the similarity of the slopes with asteroids of the same class.

4. Discussion

We will first discuss taxonomy of the present asteroids, which will lead us to stress the importance of continuum slopes in both asteroid taxonomy and characterization. We will then present our data in the form of continuum plots, looking at individual C complex asteroids, individual X complex asteroids, and then comparing the C and X fields. We will then discuss the terrestrial phyllosilicate data reported by Ostrowski et al. (2010), and the C chondrites, suggesting asteroid linkages where possible. Finally we offer some thoughts on the nature of C and X complex asteroids.

4.1. Taxonomy of the present asteroids and the importance of continuum slope

The classifications of the present asteroids are shown in Table 3. In general, we have taken these classes assignments from the literature but where necessary we used the DeMeo et al. (2009) on-line software (http://smass.mit.edu/cgi-bin/busdemeoclass-cgi). As mentioned above, Principal Components Analysis finds that continuum slope, absorption at ~0.8 μm, and absorption in the UV were the major factors cause of variation and the resulting classes are described in Table 4. For five of the nine classes an absorption feature is part of the class description, but for all nine continuum slope is also part of the class description with slope increasing along the B-C-X series. The evolution in taxonomy between the first Tholen (1989) and Bus and Binzel (2002) schemes in Table 3 is significant, but only five of our asteroids (numbers 24, 51, 88, 129 and 7753) needed reclassification on the basis of the additional near-IR data.

4.2. Existing data for absorption features in the spectra of these asteroids

In Table 5 we report data for spectral features in the present asteroids using literature parameters for identifying water-related features. We calculated parameters for UV absorption, the depth of absorption at 0.7 μm, and the depth of absorption at 3 μm. As with previous workers (Vilas, 1994; Hiroi et al., 1996; Hiroi and Zolensky, 1999; Fornasier et al., 1999), we measure these absorptions with three ϕ parameters, ϕ_{UV}, (UV absorption strength), $\phi_{0.7}$ (0.7 μm band strength) and ϕ_3 (3 μm band strength) which are defined by:

$$\phi_{UV} = \ln R_{0.337} - \ln R_{0.550}$$
$$\phi_{0.7} = \ln R_{0.701} - [0.152 \ln R_{0.550} + 0.151 \ln R_{0.853}]/0.303$$
$$\phi_3 = \ln R_{\sim 3.0} - \ln R_{\sim 2.4}$$

where R refers to spectral reflectance and the subscripts refer to wavelength in μm. In a few cases where data are not available at 0.337 μm, we use the lowest wavelength available, 0.443 μm. A few test cases showed this was acceptable, since this part of the spectrum was usually linear.

Judging from the plots of Hiroi et al. (1996; their Fig. 4) and the spread in positive values in Table 5, we take the presence of a water-related feature to be indicated if $\phi_{UV} < -0.3$, if $\phi_{0.7} < 0.01$ (assuming this feature is water-related, Vilas, 1994), and if $\phi_3 < -0.02$. The ECAS and SMASS data produce slightly different results for the 0.7 μm feature because of the higher resolution for the SMASS spectra, but not enough to significantly affect our analysis. We find evidence for water-related features in 10 out of 15 of the

Table 5
Spectra data on the present asteroids and water-related features.[a]

Asteroid		Absorption/bands calculated value			Evidence for water?			Refs.[b]
Number	Name	UV (ϕ_{UV})[c]	0.7 μm ($\phi_{0.7}$)[c]	3 μm (ϕ_3)[c]	UV absorption[d]	0.7 μm band[d]	3 μm band[d]	
24	Themis	−0.2220	−0.0071	−0.0652	N	Y	Y	1, 5, 7
34	Circe	−0.2303	−0.0259	nd	N	Y	nd	1, 2, 5
45	Eugenia	−0.0953	0.0138	nd	N	N	nd	1, 4, 5
51	Nemausa	−0.4664	−0.0213	−0.6279	Y	Y	Y	1, 5, 6
52	Europa	−0.1262	0.0265	0.0269	N	N	N	1, 5, 6
77	Frigga	−0.1253	0.0298	−0.0741	N	N	Y	1, 4, 5
87	Sylvia	−0.0712	−0.0017	−0.0050	N	Y	N	1, 5, 7
88	Thisbe	−0.1299	−0.0085	(0.5503)	N	Y	Y	1, 2, 5, 6
93	Minerva	−0.1874	0.0037	nd	N	Y	nd	1, 5
129	Antigone	−0.0249	0.0275	−0.1221	N	N	Y	1, 4
140	Siwa	−0.0839	0.0292	nd	N	N	nd	1
181	Eucharis	−0.0231	0.0435	nd	N	N	nd	1
191	Kolga	0.0213	−0.4869	nd	N	Y	nd	1
213	Lilaea	−0.0083	−0.0060	nd	N	Y	nd	1, 5
3691	Bede	−0.1656	0.0234	nd	N	N	nd	3

[a] Excluded are Asteroids 7753 (1988 XB) and 153591 (2001 SN263) for which there are no data at these wavelengths. "N" indicates no, "Y" indicates yes, "nd" indicates no data for these features.

[b] References and spectral ranges as follows: 1. Bus and Binzel (2002); SMASS (0.435–0.925 μm). 2. Xu et al. (1995) (0.5099–1.0078 μm). 3. Binzel et al. (2004) (0.435–0.925 μm). 4. Rivkin and Neese (2003) (1.9–3.6 μm). 5. Zellner et al. (1985) (0.337–1.041 μm). 6. Jones et al. (1990) (1.25–3.73 μm). 7. Feierberg et al. (1985b) (2.3–3.5 μm).

[c] Slopes and band strengths (ϕ values) defined as follows: $\phi_{UV} = \ln R_{0.337} - \ln R_{0.550}$ $\phi_{0.7} = \ln R_{0.701} - [0.152 \ln R_{0.550} + 0.151 \ln R_{0.853}]/0.303$ $\phi_3 = \ln R_{\sim 3.0} - \ln R_{\sim 2.4}$, where R is spectral reflectance and the subscripts refer to wavelength (μm).

[d] Water is assumed to be present if the UV slope smaller than −0.3, if the 0.7 μm band is less than 0.01, and if the 3 μm band is smaller than −0.02 (see text for explanation).

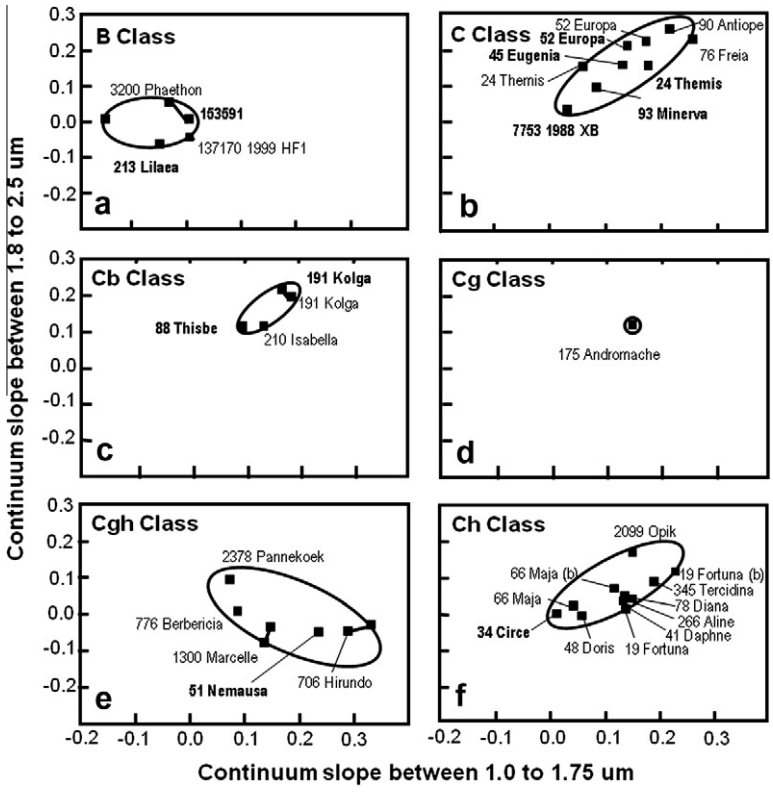

Fig. 4. Continuum plots for asteroids in the C complex, with a panel for each class. Present data in bold type, literature data in normal type. In most cases, the class members define fairly narrow fields on this plot, usually with a positive trend, especially where the number of observations is four or greater. Note that where there are two observations by different research groups, in general the agreement between groups is very good. The literature data is taken form SMASS-Small Main-Belt Asteroid Spectroscopic Survey, Binzel et al. (2004) and MIT-UH-IRTF Joint Campaign for NEO Spectral Reconnaissance.

spectra of the present asteroids. On the other hand, all three features are present in the spectra of only one of the present asteroids, namely 51 Nemausa.

Vilas (1994) found that 47.7% of C asteroids, 33.0% of B asteroids, and 5.6% of X asteroids showed evidence for hydration. We find that eight out of the 15 for which we have data show an absorption feature at 0.7 μm. Four of the present asteroids were included in the Vilas (1994) study. Vilas found 0.7 μm and 3.0 μm features in the 51 Nemausa spectra, and none for 52 Europa, in agreement with the present results, but she found neither band in 87 Sylvia (we find a 0.7 μm band), and while we find both bands in 88 Thisbe, she found only the 0.7 μm band. In other words, while

there is a high degree of agreement over the objects as a whole, there are differences at the individual object level.

Features seen at <0.55 μm (in the Xe class) and 0.8–1.0 μm (in the Xk class) are diagnostic of their classes and might be associated with hydration features (Rivkin et al., 2002) while the absorption band >1 μm sometimes seen in class Xk could be associated with olivine and pyroxene (Sunshine and Pieters, 1993).

4.3. Continuum plots for individual C complex asteroids

Fig. 4 shows continuum plots for the C complex asteroids in the present study augmented by literature data where available (Table 6). There are many instances of good-to-excellent agreement between separate observations in well-populated classes. Apparently, continua slopes can be reproducibly determined and that this method of quantifying the spectra is meaningful. Second, the B class plots to the left of the C classes, and the C class generally plots higher than the other classes. Third, the C, Cb and Ch classes display positive correlations between the long-wavelength slope and short-wavelength slope (with slopes on this plot of 1.0, 1.1 and 0.6, respectively). On the other hand, the B and Cgh class produce either horizontal or slightly negative trends. The Cb and Cg classes, with four or less members, are not well defined. We will now discuss each class in turn.

Table 6
Literature data for continuum slopes and albedos for C and X asteroids.

Asteroid	Class	Short λ slope	Long λ slope	Albedo*
16 Psyche	Xk	0.192 ± 0.002	0.167 ± 0.009	0.1203
19 Fortuna	Ch	0.135 ± 0.003	0.030 ± 0.007	0.037
19 Fortuna[b]	Ch	0.227 ± 0.003	0.111 ± 0.008	0.037
21 Lutetia	Xc	0.115 ± 0.007	0.022 ± 0.001	0.2212
22 Kalliope	X	0.281 ± 0.005	0.177 ± 0.006	0.1419
24 Themis	C	0.054 ± 0.002	0.169 ± 0.005	0.067
41 Daphne	Ch	0.131 ± 0.003	0.039 ± 0.004	0.0828
48 Doris	Ch	0.056 ± 0.001	−0.002 ± 0.007	0.0624
52 Europa	C	0.168 ± 0.003	0.223 ± 0.007	0.0578
55 Pandora	Xk	0.285 ± 0.005	0.228 ± 0.006	0.3013
55 Pandora[b]	Xk	0.267 ± 0.012	0.207 ± 0.01	0.3013
66 Maja	Ch	0.042 ± 0.002	0.013 ± 0.002	0.0618
66 Maja [b]	Ch	0.109 ± 0.003	0.071 ± 0.009	0.0618
69 Hesperia	Xk	0.293 ± 0.003	0.219 ± 0.006	0.1402
76Freia	C	0.253 ± 0.004	0.247 ± 0.007	0.0362
77 Frigga	Xe	0.167 ± 0.001	0.056 ± 0.003	0.144
78 Diana	Ch	0.135 ± 0.006	0.069 ± 0.006	0.0706
87 Sylvia	X	0.248 ± 0.004	0.250 ± 0.007	0.0435
90 Antiope	C	0.212 ± 0.006	0.270 ± 0.006	0.0603
99 Dike	Xk	0.099 ± 0.006	0.004 ± 0.005	0.0627
110 Lydia	Xk	0.270 ± 0.002	0.213 ± 0.004	0.1808
132 Aethra	Xe	0.121 ± 0.004	0.017 ± 0.006	0.199
153 Hilda	X	0.261 ± 0.006	0.187 ± 0.006	0.0618
175 Andromache	Cg	0.146 ± 0.005	0.111 ± 0.004	0.0819
191 Kolga	Cb	0.177 ± 0.002	0.201 ± 0.003	0.0408
210 Isabella	Cb	0.132 ± 0.001	0.113 ± 0.002	0.0436
261 Prymno	Xk	0.187 ± 0.003	0.137 ± 0.006	0.1141
266 Aline	Ch	0.147 ± 0.001	0.042 ± 0.004	0.0448
345 Tercidina	Ch	0.187 ± 0.002	0.097 ± 0.006	0.0654
706 Hirundo	Cgh	0.319 ± 0.003	−0.020 ± 0.008	0.1721
706 Hirundo [b]	Cgh	0.293 ± 0.005	−0.041 ± 0.009	0.1721
776 Berbericia	Cgh	0.085 ± 0.002	0.010 ± 0.005	0.0655
1300 Marcelle	Cgh	0.129 ± 0.007	−0.070 ± 0.007	0.0995
1300 Marcelle [b]	Cgh	0.145 ± 0.008	−0.031 ± 0.003	0.0995
2099 Opik	Ch	0.144 ± 0.005	0.161 ± 0.003	
2378 Pannekoek	Cgh	0.072 ± 0.004	0.079 ± 0.006	0.0891
3200 Phaethon	B	−0.165 ± 0.008	0.007 ± 0.009	0.1066
3691 Bede	Xc	0.143 ± 0.005	−0.016 ± 0.004	
53319 1999JM8[a]	X	0.156 ± 0.009	0.164 ± 0.007	
137170 1999 HF1	B	−0.001 ± 0.004	−0.034 ± 0.009	

[a] Corrected for thermal radiation.
[b] Duplicate observation.
* Albedo data from Chamberlin and Yeomans (2010).

There are five members of the B class in Fig. 4a, with duplicate observations for one that are in reasonable agreement. One of the asteroids at the lower end of the range is 3200 Phaethon, which is thought to be the parent of the Geminid meteor stream and an extinct cometary nucleus (Ohtsuka et al., 2006). Asteroid 137170 1999 HF1 shows a second periodicity in the light curve indicating that it is a binary object (Polishook and Brosch, 2008). Asteroid 153591 is a near-Earth asteroid that is actually a triple system, the first reported among the NEA (Nolan et al., 2008).

There are nine members of the C class (Fig. 4b) and we have two independent observations of 24 Themis and 52 Europa. The duplicate data for 52 Europa are in good agreement, but the short-wavelength slopes of the two spectra for 24 Themis spread across the ellipse in weak agreement. Asteroid 90 Antiope is a double asteroid in the Themis family (Descamps et al., 2007) and plots near the upper end of the range. Asteroid 93 Minerva is a large main-belt asteroid that plots at the lower end of the range. Of the C asteroids that were observed for this study, only 24 Themis has significant data for hydration with both a 0.7 μm feature and a 3 μm feature (Table 5). For Asteroids 45 Eugenia, 52 Europa, and 93 Minerva, none have significant absorption features according to the criteria in Table 5. Minerva does have a weak 0.7 μm feature.

For the Cb class (Fig. 4c), the two independent observations of 191 Kolga are in good agreement. Using the criteria in Table 5, neither 191 Kolga and 88 Thisbe have detectable UV absorption features in our data. Asteroid 191 Kolga has a fairly strong 0.7 μm feature, which would normally be indicative of Ch or Cgh asteroids. However, the continuum slopes strongly supports the Cb classification, though it also plots on the edge of the upper left boundary of the Ch field (compare Fig. 4c with Fig. 4e and f).

For the Cg asteroids (Fig. 4d) we have only one object (175 Andromache) and can say little, other than observe that it provides some indication of the location of the field.

For the Cgh class (Fig. 4e), we have seven observations including duplicates for 706 Hirundo and 1300 Marcelle. There is excellent agreement between the observations of the duplicates. The other members of the group are 51 Nemausa, 776 Berbericia, and 2378 Pannekoek. Asteroid 51 Nemausa was mentioned above since it is anomalous in Fig. 3, a reflection of its unusual spectrum in which a large positive slope changes abruptly at ~1.5 μm to a shallow or negative slope (Fig. 1). The clustering in Fig. 4e suggests that this behavior is typical of the class. Asteroid 51 Nemausa has rotational spectral variations suggesting a non-uniform surface composition (Sawyer, 1991), and that its surface contains a "red spot" (Kristensen, 1991). Asteroid 51 Nemausa does has a 0.7 μm feature in its spectrum, but also as mentioned above it shows a strong UV absorption and 3 μm feature (Table 5). This is in agreement with Hiroi et al. (1996) who found a positive correlation between the UV absorption and 3 μm feature. Apparently, 51 Nemausa has water in some form on its surface.

The Ch asteroid field is well populated with 11 members and a fairly well defined ellipse (Fig. 4f). Asteroid 2099 Opik stands slightly apart from the others because its near-infrared spectrum is a steadily increasing continuum, whereas other Ch asteroids level off at longer wavelengths. Maybe the classification of 2099 Opik should be reconsidered. The Ch class is defined by having members with a 0.7 μm feature, but the only Ch asteroid we observed, 34 Circe, has a 0.7 μm feature and no UV absorption (Table 5). The two data points based on literature spectra for Asteroid 19 Fortuna have weak agreement in the short and long-wavelength slopes because of about a 0.7 separation on both axes.

4.4. Continuum plots for individual X complex asteroids

Fig. 5 shows the present and literature data for the four classes in the X complex consisting of the X, Xc, Xe and Xk classes. Again

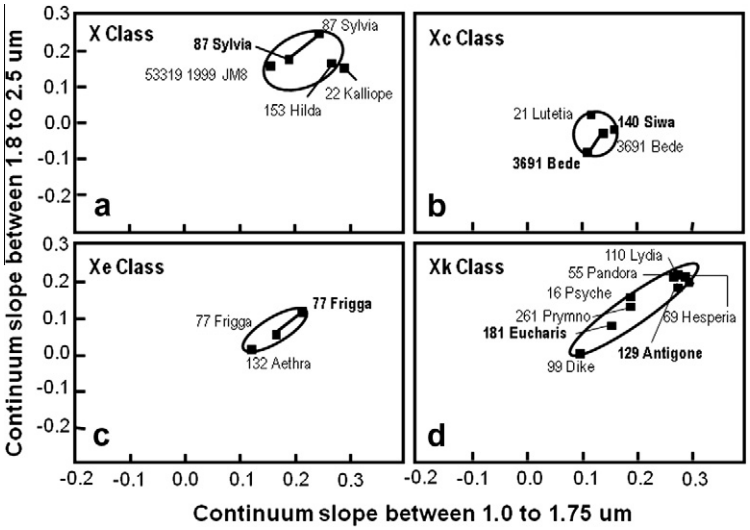

Fig. 5. Continuum plots for asteroids in the X complex. Details as in Fig. 4. Again there is fairly tight clustering, positive slopes, and good agreement between observers.

there are many cases of very good agreement between duplicate observations of the same asteroid (two observations are generally within ~0.07 on each axis): 87 Sylvia, 3691 Bede, 77 Frigga, and 55 Pandora, for example. Second, except for the Xc class (for which there are few objects), the trends on these plots are positive. The slopes for the trend lines in Fig. 5 are 0.6, 0.8 and 1.1 for the X, Xe and Xk classes, respectively, similar to the values the C complex mentioned above. We will now discuss each class individually.

There are four members of the X class (Fig. 5a), 153 Hilda, 53319 1999 JM8, 22 Kaliope and 87 Sylvia. Our spectrum for 87 Sylvia contained no water-related spectral features (Table 5), but a 0.7 μm was been observed by Zellner et al. (1985). The three members of the Xc class, 3691 Bede, 140 Siwa, and 21 Lutetia, plot closely in Fig. 5b. 3691 Bede is a tumbling asteroid (Pravec et al., 2005), which might explain the small differences in the two observations. According to our criteria there are no water-related features in the spectra of Xc Asteroids 140 Siwa and 3691 Bede (Table 5). The Rosetta spacecraft will flyby Lutetia in 2010 and Lazzarin et al. (2004) have observed features attributed to aqueous alteration in the spectra of the surface. The two members of the Xe class (Fig. 5c) plot close to each other. Asteroid 77 Frigga does not appear to have UV absorption or 0.7 μm, but does have a 3 μm feature (Table 5). The Xe Asteroid 132 Aethra is noted for its relatively flat spectrum, especially in the long wavelengths. Finally, the eight members of the Xk class form a reasonably tight cluster with steep continuum at both the short and long wavelengths (Fig. 5d). Asteroids 129 and 181 Eucharis do not to have a 0.7 μm feature and UV absorption according to our criteria, but a weak 3 μm feature is present in the spectra of 129 Antigone.

4.5. Comparison of C and X fields

The ellipses drawn around the fields in Figs. 4 and 5 are compared in Fig. 6. Three points can be stressed, some of which were mentioned above and have been noted by others. First, in general, the X complex classes are displaced to the right on Fig. 6 relative to the C complex classes and the B asteroids are displaced to the left. In other words, the (1) members of the X complex tend to have similar continua in the long wavelength range but steeper continua in the short wavelength range compared to the C complex, and (2) B asteroids have smaller (negative) slopes at short wavelengths but among the shallower slopes at long wavelengths compared to the rest of the C complex and the X complex asteroids. The major

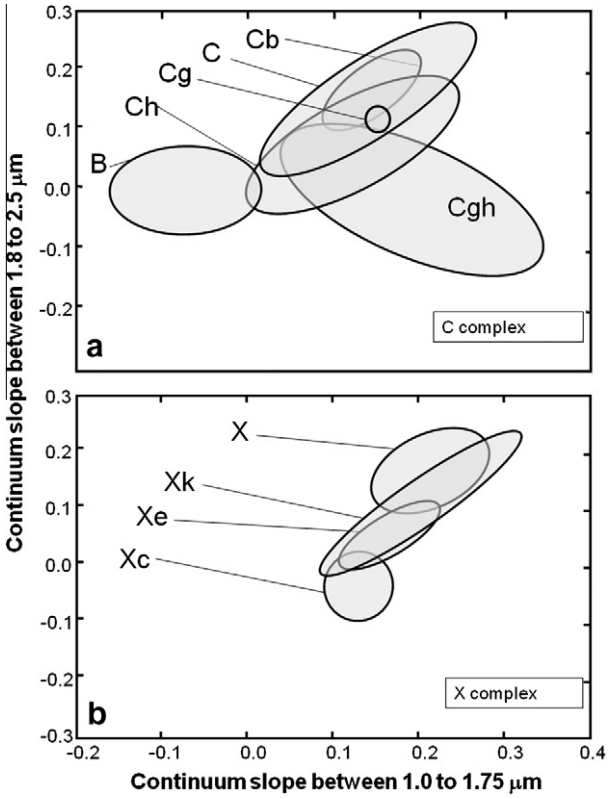

Fig. 6. Summary of the fields identified in Figs. 4 and 5. The prevalence of positive slopes and the difference between the C and X complexes in overall slope on these plots are apparent. (See also Fig. 3.) Most particularly, the X complex classes are displaced to the right relative to the C complexes. These plots provide a means of comparing asteroid spectral reflectivity data with that of other similar samples, such as heated phyllosilicates and C chondrites.

exception is that the Cgh class overlaps with the X complex. Second, while slopes of the X complex classes are very similar (notwithstanding the small number and clustering of the Xc class), the C complex classes show a wide range of behavior with some classes having similar trend slopes to the X complex classes.

While there is some overlap of the fields shown by the various asteroid classes, it is clearly not close to 100%. In fact, the overlap of

one class with its closest neighbor is usually <50%. Thus the classes recognized on the basis of spectra in the visible and infrared range are reflected in these continua plots lending an additional indication that such continuum plots are meaningful. These plots provide a quantitative basis for comparing astronomical data with laboratory data, such as data for meteorites and terrestrial phyllosilicates, providing certain issues can be satisfactorily dealt with.

4.6. Considerations when comparing laboratory measurements with astronomical measurements

In comparing laboratory measurements with astronomical measurements we are concerned with three primary effects. (1) The similarity of the standard light sources for the laboratory and astronomical measurements. In the case of the laboratory spectrometer, the reference light source is a halogen lamp whereas for the astronomical measurements the reference light source is a number of solar-like stars. (2) The effect of grain size on the measurements and how the grains used for laboratory measurements compare with grains sizes on the asteroids. (3) Laboratory measurements are made on freshly ground interior samples, while astronomical measurements are made on a surface that has been exposed to space. In space, there will have been a number of alteration processes (impact, micrometeorite erosion, solar wind implantation, solar energetic particle interactions, thermal cycling, for example) that are collectively referred to as "space weathering".

In response to point (1), our laboratory light source is normalized to a white spectral-standard material (TiO_2). The stellar reference sources may not be perfectly white, but they are close, and any error caused by slight differences is well within our experimental uncertainties, especially since the range of slopes we observe in the asteroid, meteorite, and mineral spectra are very large.

In response to point (2), Fig. 7 shows the continuum plot for samples of Murchison of three sieve fractions, the data being those of Gaffey, Hiroi, and Pieters taken from the RELAB database. The range of slopes in the short wavelength interval is considerable, with data ranging from −0.1 to 0.5 on the horizontal axis with slope decreasing with coarsening grain size. On the other hand, the range of slopes in the longer wavelength interval is small or negligible. The data shown in Fig. 7 are surprising, since, in general, data for a given meteorite or meteorite class tends to be very reproducible, regardless of grain size. Fig. 8 shows the continuum plot for meteorites for which near-IR spectra have been published. The data appear in Table 7. Five CM chondrites plot in the same general region of the continuum plot, having relatively steep positive slopes in the 1.0–1.75 μm region, and no overlap with the remaining meteorites. In fact, three CM chondrites (Cold Bokkeveld, Murray and Murchison) are the same within experimental uncertainties. Three CI/CM chondrites have similar slopes to the CM chondrites in the 1.8–2.5 μm region, but significantly shallower slopes in the 1.0–1.75 μm region. Three C remaining chondrites, CV, CR, and CK chondrites, have 1.0–1.75 μm slopes of 0.05–0.20 but negative slopes in the long wavelength region. In other words, the continuum plot is separating these three types of C chondrite. This suggests that these data are not being dominated by grain size effects and can be compared with asteroid data.

An exception is the CI chondrites where there is evidence of considerable variation in the slopes of their continua. There is poor agreement for Orgueil in the spectra obtained by Gaffey and Hiroi and there is poor agreement between the two splits of Ivuna run by

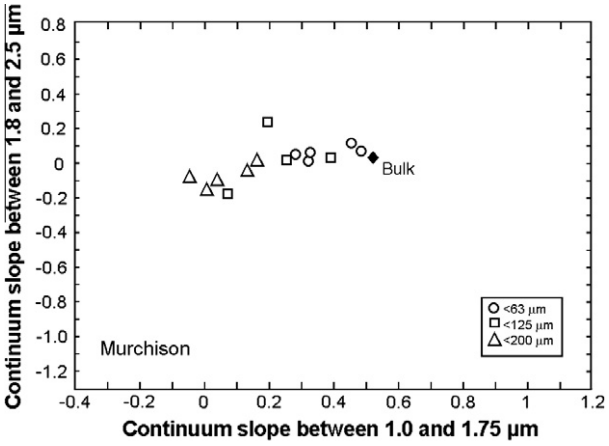

Fig. 7. Continuum plot for bulk and grain separates of samples of the Murchison CM chondrite. The Murchison bulk data point is from Hiroi et al. (1993, 1996) while the grain size fractions are from spectra acquired by Mike Gaffey, Taki Hiroi, and Carle Pieters at the NASA RELAB Laboratory at Brown University. While grain size seems to affect the continuum slope at the shorter wavelengths, there is little or no effect on the continuum slope at the longer wavelengths. The finer grain fractions (<63 and <125 μm) plot in the CM chondrite field while the coarser fraction (<200 μm) plot in the C asteroid field.

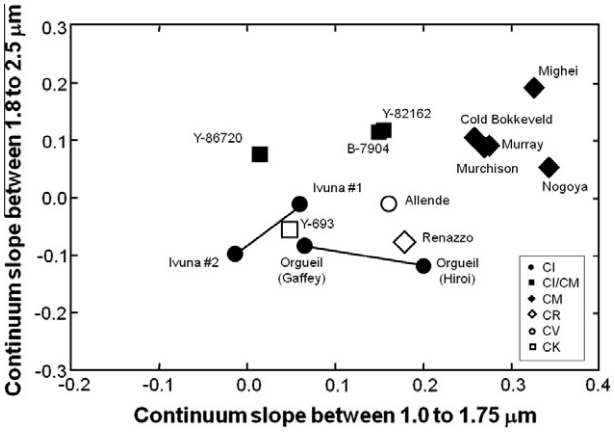

Fig. 8. Continuum plot for fifteen C chondrites. The data for the C chondrites is from Table 7. The chondrites plot in the same general vicinity of the plot as the C and X asteroids (Fig. 6), but with significant differences in detail. CM chondrites plot in the upper right of this diagram, CI/CM chondrites in the upper middle, and the remainder (CI, CV, CR and CK) plot in the middle lower region of the plot. This suggests that continuum slopes have taxonomic (genetic) value, and are a basis of comparison with terrestrial minerals and asteroids.

Table 7
Continuum slopes and albedos of carbonaceous chondrites.

Meteorite class	Meteorite name	Short slope	Long slope	Albedo[a]
CI/CM	Y-86720	0.004 ± 0.0002	0.090 ± 0.005	
CI/CM	B-7904	0.141 ± 0.007	0.128 ± 0.006	
CI/CM	Y-82162	0.150 ± 0.007	0.129 ± 0.006	
CK	Y-693	0.038 ± 0.002	−0.040 ± 0.002	
CV	Allende	0.153 ± 0.008	0.006 ± 0.0003	0.102
CR	Renazzo	0.168 ± 0.008	−0.060 ± 0.003	
CI	Ivuna #1	0.044 ± 0.002	−0.017 ± 0.0008	
CI	Ivuna #2	−0.018 ± 0.0009	−0.080 ± 0.004	
CI	Orgueil (Hiroi)	0.193 ± 0.010	−0.104 ± 0.005	0.072
CI	Orgueil (Gaffey)	0.052 ± 0.002	−0.069 ± 0.003	0.072
CM	Mighei	0.316 ± 0.003	0.199 ± 0.008	0.051
CM	Cold Bokkeveld	0.259 ± 0.001	0.115 ± 0.005	
CM	Murray	0.268 ± 0.001	0.103 ± 0.005	
CM	Murchison	0.263 ± 0.004	0.094 ± 0.007	0.061
CM	Nogoya	0.335 ± 0.006	0.071 ± 0.004	0.051

[a] Zellner et al. (1977).

Hiroi. Nevertheless, they still plot in a region discrete from the CM and CI/CM chondrites with shallow 1.8–2.5 μm slopes. The reason for the poor agreement between splits is the very likely due to the large amount of water in these meteorites that can easily be lost during handling.

One caveat in comparing data for grain size separates with asteroid data is that the asteroid surfaces are probably dominated by pebble to boulder sized particles so the data in Fig. 7 probably have little relevance to the issue. These spacecraft observations of different surfaces on asteroids tend to give very similar spectra regardless of texture also suggesting that grain size is not driving spectral slopes. For example, the Eros "ponds" are very fine grained and the remainder of the surface is very rough, yet their spectral slope differences are less 4% (McFadden et al., 2001). Similarly, the Muses Sea on Itokawa shows a ~10% differences in albedo and band depth compared to the surrounding much rougher regions, but the slope shows little or no change (Abe et al., 2006). Eros and Itokawa are S complex asteroids, where one might expect grain size effects because of their expected petrologic complexity. The C complex asteroids, if they are similar to the C chondrites, are fine grained and relative homogeneous, and one would not expect major effects due to grain size.

The term "space weathering" includes all of the many processes that alter the surface of an airless body in the space environment. Most information comes from detailed investigations of lunar samples where the chief cause of changes is impact (e.g. McKay et al., 1991). On the largest scales, impact causes heating, melting, lithification, brecciation, and gardening. On the smallest scale, micrometeorite impact causes impact pits, volatilization, and glass formation, and in the process of dispersal the glass becomes agglutinates (Keller et al., 1999; Pieters et al., 2000). At the same time, solar wind exposure causes the implantation of ions and surface radiation damage (Nichols et al., 1994). The effects are therefore numerous and complicated, and extrapolation from the Moon to the asteroids is not a trivial exercise (McKay et al., 1991).

Gas-rich breccia meteorites, the equivalent of lunar regolith and breccias, have a few similarities and many differences from their lunar equivalents (Keil, 1982). To some extent we can bridge the gap with laboratory experiments using lasers and charged particles (Sasaki et al., 2002; Dukes et al., 1999), observations on gas-rich regolith breccia chondrites (Britt and Pieters, 1994), and spacecraft observations of asteroids (Chapman, 1996). Clark et al. (2002) recently reviewed the overall effects of space weathering on asteroid reflectance spectra, pointing out that reddening and neutral darkening will happen, but that the degree of reddening is much less than for lunar samples.

Space weathering always has to be borne in mind when comparing astronomical and laboratory data, but it seems to us that the effects will be small compared to the class-to-class variations for asteroids and meteorites. In any event, if the major process distinguishing certain classes, say the S-Sq-Q sequence, as advocated by Binzel et al. (1996), is space weathering, then by studying these classes we are implicitly investigating space weathering.

4.7. Comparison of C and X fields with terrestrial phyllosilicate fields

It is frequently assumed, based on mineralogical studies of meteorites, that the surfaces of C asteroids consist of phyllosilicates (e.g. Rivkin et al., 2002). There are several spectral features that are consistent with this, such as the presence of water features at 3 μm and other wavelengths and a feature at 0.7 μm attributed to Fe^{2+} to Fe^{3+} charge transfer, which might occur in a hydrated environment (Vilas and Gaffey, 1989). However, these features are very weak, certainly much weaker than observed in terrestrial phyllosilicates in the laboratory. The reason for the almost featureless spectra of asteroids must be associated with their space environment, exposure to the vacuum of space, solar irradiation effects, micrometeorite and meteorite impact effects. Thus the immediate surface has seen a high temperature history and dehydrated surfaces are to be expected. Thus Hiroi and Zolensky (1999) and Ostrowski et al. (2010) have compared the spectra of asteroids to those of phyllosilicates heated in the laboratory. The effects are particularly apparent in the heating experiments of Ostrowski et al. (2010), where temperatures in excess of 700 °C were employed.

Fig. 9 is a continuum plot that compares the present C and X asteroid complexes with terrestrial phyllosilicates that have been heated to >700 °C (Ostrowski et al., 2010). Data for five terrestrial phyllosilicates are shown, which bracket the large range of structures and compositions found in terrestrial phyllosilicates and include the phyllosilicates observed in meteorites. Upon heating, absorption bands in the near-IR spectra of phyllosilicates weaken and eventually disappear while continua increase in slope, especially at longer wavelengths where a number of major water-related absorption bands occur (Ostrowski et al., 2010). At ~700 °C chemically bound water is lost and the phyllosilicate lattice collapses. The decomposition products depend on the phyllosilicate, and consist of a few identifiable minerals in a mostly amorphous matrix. However, the spectra of the dehydrated phyllosilicates show little overlap on the continuum plots, especially in the long wavelength interval.

The fields for the asteroid complexes overlap with the fields for heated kaolinite, montmorillonite, and serpentine. Nontronite and chlorite occupy regions of Fig. 9 with steeper long wavelength continuum slopes. This is especially interesting in the case of chlorite, which has occasionally been observed in C chondrites. On the basis of Fig. 9 we suggest that the prominent minerals in the surface material of C complex asteroids resemble the decomposition products of heated kaolinite and montmorillonite. Montmorillonite has been observed in C chondrites, but kaolinite is a surprise. In terrestrial occurrences kaolinite is an aqueous alteration product of feldspar, which is found in small amounts in ordinary chondrites but not in carbonaceous chondrites. Perhaps some of these asteroids were once feldspar- and water-rich. Montmorillonite is formed by aqueous alteration of olivine and pyroxene, common meteorite-forming minerals, in alkaline aqueous conditions.

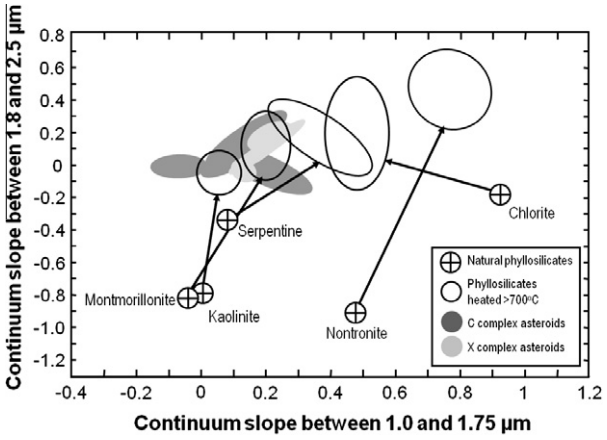

Fig. 9. Continuum plot comparing terrestrial phyllosilicates with fields for heated phyllosilicates, and the C and X complex asteroids. Phyllosilicate data from Ostrowski et al. (2010), asteroid complex fields summarize the data in Fig. 6. The original location of the phyllosilicates appear as crossed-circles while the area occupied by the samples heated to 700 and 1100 °C are indicated by ellipses with arrows connecting the two. On the basis of this plot we infer that the C complex contains portions of the heated kaolinite and heated montmorillonite and the X complex asteroids contain heated montmorillonite and possibly serpentine.

The X complex overlaps the heated montmorillonite field and touches the field for heated serpentine (Fig 9). As mentioned above, the past presence of montmorillonite on an asteroid surface seems reasonable, as does the presence of serpentine. Serpentine has frequently been observed in carbonaceous chondrites.

4.8. Comparison with meteorites

The C chondrite classes plot in the same general region of the continuum plot as the C and X complex asteroids (Fig. 10). However, there are several interesting points to make.

First, the CM chondrites do not fall into any of the C complex fields and while they are close to several X fields they also fall to the right of the X classes.

Second, the CI chondrites do not plot in any of the X fields but plot in the same general area of the diagram as B, Ch, and Cgh fields.

Third, the CR, CV, and CK chondrites are close to the Ch field but plot in the Cgh field. Allende also plots on the Xc field.

Finally, the three CI/CM chondrites plot close to several C asteroid fields (i.e. Cg, Cb, Ch, and C), and two CI/CM chondrites plot close to the X and Xk classes. However, all three CI/CM chondrites plot in the C asteroid field. A relationship with the Ch class can be ruled out because Y-86720, Y-82162 and B-7904 do not have a 0.7 μm feature (Hiroi et al., 1996).

Based on the low albedo and essentially featureless spectra with occasional 0.7 μm and 3 μm features, that CM chondrites have been linked to C complex asteroids, the Ch asteroids especially (Fornasier et al., 1999; Burbine, 1998; Burbine et al., 2002). However, the continuum plot suggests a closer affinity for CM chondrites to the X complex asteroids than the C complex asteroids. This is illustrated with the raw spectra in Fig. 11. Below 0.9 μm there is good match between the spectra of the meteorite and the asteroids. However, at longer wavelengths there are significant differences between the spectra for the two C asteroids, 19 Fortuna (Ch) and 175 Andromache, and the CM chondrite Cold Bokkeveld. In contrast, the spectra for two X complex Asteroids 110 Lydia (Xk), and 153 Hilda (X) match closely the spectrum for Cold Bokkeveld, the only discrepancy being a slight negative slope short of 0.85 μm for Cold Bokkeveld.

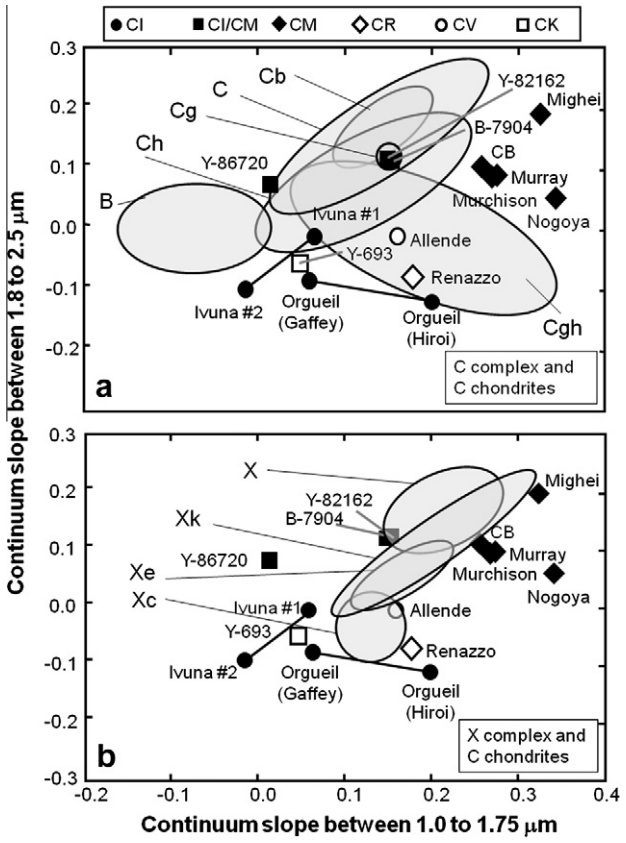

Fig. 10. Continuum plot comparing the C chondrites (data from the NASA PDS database; Gaffey, 2001) with the asteroid fields. (a) C chondrites compared C complex asteroids (b) the C chondrites compared with X complex asteroids. Based on these figures and other data discussed in the text we suggest associations between the C chondrites and the asteroid classes as listed in Table 8.

In Table 8, we list the meteorite–asteroid associations we would propose on the basis of the continua in the near IR. Two of the three meteorites classified as CI/CM plot in or near the Cb, Cg, and C fields, while the third plots between the C and B fields. If we assume that all three CI/CM chondrites should come from the same parent source, then we would favor the C class as it is equally suited to all three chondrites. Y-693 is placed to be equally associated with the Ch and Cgh classes. The two chips of the Ivuna CI chondrite could be linked with the B, Ch, or Cgh asteroid classes, while the two chips of the Orgueil CI chondrite are closest to the Cgh asteroid field. If we use the argument members of a single class should be linked with the same asteroid then we would have to link all the CI chondrites with the Cgh class. Renazzo also plots in the Cgh field, so a linkage with the CI chondrites might be implied, but it also plots with the Xc field which is an equally likely match that would separate it from the CI chondrites. There are many petrographic and compositional differences between Renazzo and the CI chondrites. Allende also plots with the Cgh and Xc asteroids, but it lacks any similarity with CI chondrites and has been linked with the CV chondrites, which makes a linkage with Xc asteroids likely. The CM chondrites were discussed above. While they do not plot in any of the asteroid fields they are closest to Xk and if we assume all CM chondrites came from one body it would have to be an Xk asteroid. Hiroi et al. (1993) pointed out that the CM chondrites needed to be heated to make their spectra match those of C asteroids.

In addition to matching meteorite and asteroid spectra, we can compare albedos. Asteroid albedos are listed in Table 6 and the few chondrite albedos available are listed in Table 7. Asteroid classes C, Cb, and Ch have albedos of 0.04–0.07, while B, and Cg asteroids have albedos around 0.1. The Cgh asteroids show a wide range of albedos, 0.05–0.17, which is similar to the range shown by X asteroids and slightly less than the Xc (0.07–0.22) and Xk (0.06–0.30) asteroids. Xe asteroids generally have higher albedos, 0.14–0.19. In comparison, CI and CM chondrites have albedos 0.05–0.07 while CV chondrites have albedos of about 0.1. In short, in view of the variety of albedos within a given asteroid class, and the small number of asteroids and chondrites for which we have albedo data, we see no problem with the proposed matches listed in Table 8.

We now compare the mineralogies derived from reflectance spectra as summarized in Fig. 9 with the mineralogy of the C chondrite classes determined by laboratory methods. The matrix of the C chondrites is complex and fine-grained, and requires TEM, which is a highly localized technique to characterize. Current suggestions for the mineral composition of C chondrites have been summarized by Rubin (1997) and include phyllosilicates as their primary mineral. It should be stressed that much of the fine-grained material in carbonaceous chondrites appears to be a complicated mixture of Fe-rich phyllosilicates produced by aqueous alteration of metal and sulfides (as mentioned above, it is described as tochilinite, $Fe^{2+}_{5-6}(Mg,Fe^{2+})_5[(OH)_{10}S_6]$) and once referred to as PCP, "poorly characterized phase" (Barber et al., 1983; Mackinnon and Zolensky, 1984; Tomeoka and Buseck, 1985) and it is only occasionally that this phase takes on the unambiguous characteristics of a readily identifiable phyllosilicate. The matrix of CI chondrites has also

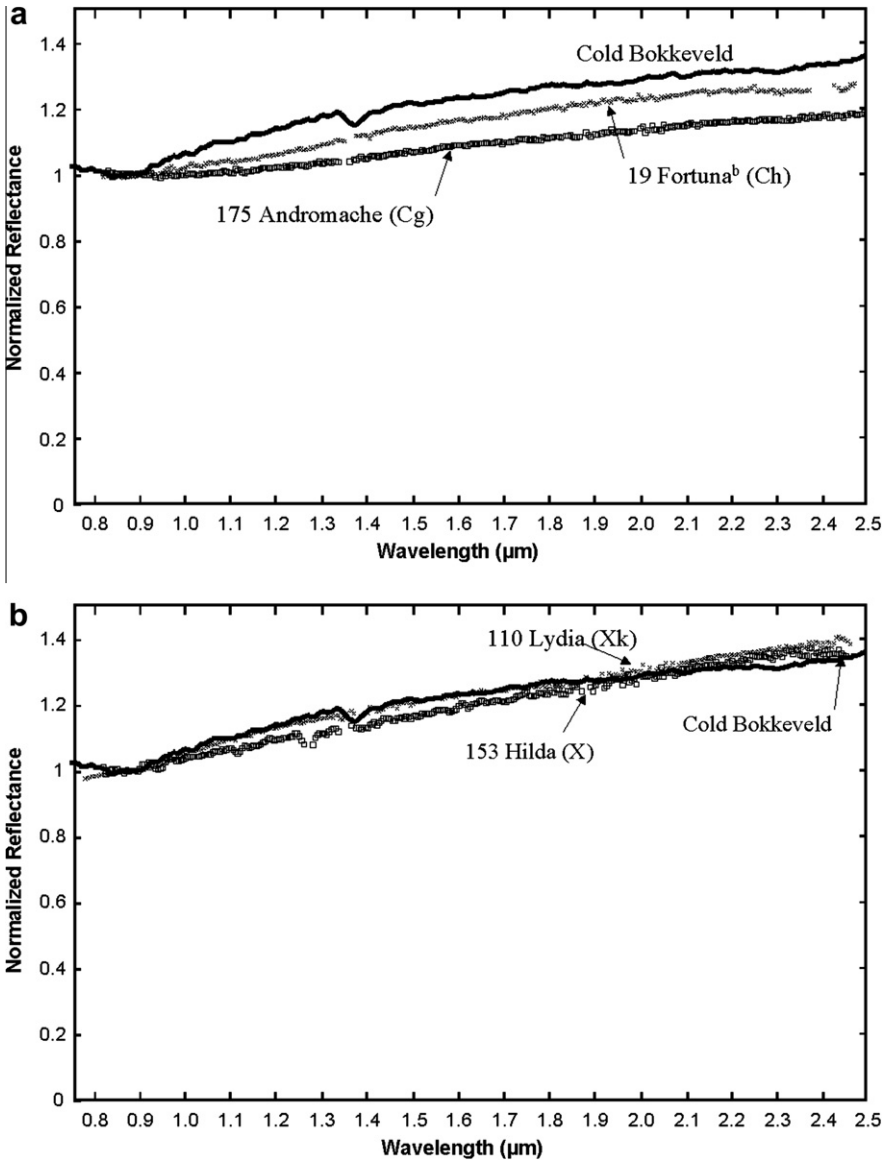

Fig. 11. Comparison of the spectra of (a) two C asteroids and the CM chondrite Cold Bokkeveld, and (b) two X asteroids and the Overlay of C asteroids and CM and X asteroids and CM chondrite Cold Bokkeveld. These spectra illustrate the differences in slope that have been described earlier in this paper and cause us to link, as an example, the CM chondrites with the Xk asteroids rather than any of the C asteroid classes.

Table 8
Meteorites considered in the present study and proposed asteroid class associations.

Meteorite name	Meteorite	Asteroid class
Y-82162	CI/CM	C
B-7904	CI/CM	C
Y-86720	CI/CM	C
Y-693	CK	Ch or Cgh
Ivuna #1	CI	Cgh
Ivuna #2	CI	Cgh
Orgueil (Gaffey)	CI	Cgh
Orgueil (Hiroi)	CI	Cgh
Allende	CV	Xc
Renazzo	CR	Xc
Cold Bokkeveld	CM	Xk
Murray	CM	Xk
Murchison	CM	Xk
Mighei	CM	Xk
Nogoya	CM	Xk

been described as serpentine or montmorillonite and that the matrix of CM chondrites is serpentine, montmorillonite, or chlorite with most minerals containing measurable Fe. Montmorillonite and serpentine are known to be present in CV classes (Rubin, 1997). We earlier postulated that C complex asteroids have surfaces containing kaolinite and montmorillonite while the X complex asteroids have surfaces rich in montmorillonite and serpentine.

In addition to these major phases, there are a host of minor phases that affect the reflectivity spectra of meteorites and presumably asteroids. These are the opaque phases, finely dispersed metal and sulfide, organics (possibly), and others. Traditionally, the effects of opaque phases are modeled by adding carbon black to the silicates and are found to lower albedo and weaken bands (Clark, 1983; Milliken and Mustard, 2007). The presence of opaque phases would lower the albedo of heated phyllosilicates in our laboratory experiments and bring them into line with the albedos of C asteroids and CI and CM chondrites (Ostrowski et al., 2010). It should be noted that the near-Earth asteroids have higher albedos than the larger main-belt asteroids. This would require less opaque phases added the heated phyllosilicates to compare to the

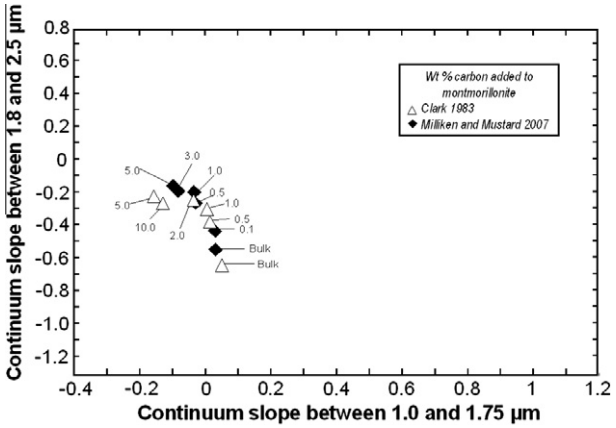

Fig. 12. Continuum plot for samples of montmorillonite to which various amounts of carbon black have been added. The addition of carbon black affects both the short and long wavelengths of the spectra, with a greater effect on the long wavelength region. In fact, the amount of carbon increases, the data show a negative linear trend in which at short wavelengths decreases from 0.0 to −0.1 while the slope at long wavelengths increases −0.6 to −0.1. This is contrast to the effect of heating on terrestrial phyllosilicates in which the trends on this plot are essentially positive (chlorite excepted).

asteroids. The effect on continuum plots is shown in Fig. 12. The data of Clark (1983) and Milliken and Mustard (2007) are in good agreement and show that the addition of opaque phases causes a relatively small decrease in the slope in the 1.0–1.75 μm region and a medium, about 0.4, increase in the slope in the 1.8–2.5 μm region, this is based on the max three weight percent in the meteorites. However, the changes are not only minor, they generally go in the wrong direction in relating terrestrial phyllosilicates to the asteroids and meteorites. We do not think that the presence of opaques is playing an important part of explaining the difference in the continuum slopes of asteroids and meteorites compared to terrestrial phyllosilicates.

4.9. On the nature of C and X complex asteroids

Phyllosilicates are highly diverse in composition and are associated with a number of discrete environments on Earth (Table 9). The weathering of feldspar-rich rock types produces kaolinite. Metamorphic and aqueous alteration of olivines and pyroxenes, typical chondritic minerals, results in serpentine, while in the presence of an Al source, such as micas, produces chlorite. In alkaline conditions and poor drainage, aqueous alteration of olivine and pyroxene rich rocks produces montmorillonite.

Asteroids with interiors resembling CI or CM chondrites may contain serpentine and chlorite from the aqueous alteration of olivines and pyroxenes, and we identify these meteorites with Cgh and Xk asteroids, respectively. Asteroids with drier interiors, through accretion at higher temperatures or small amounts of internal heating, may have CV-like interiors and would undergo aqueous alteration to produce montmorillonite, and we identify these as Xc asteroids. If kaolinite is present on the surfaces of B asteroids, as suggested by the present results, we identify no known meteorite class with them. Indeed, no meteorite class has been reported to contain kaolinite. To create the bulk composition needed to produce kaolinite, the parent asteroid would have to be differentiated, with a core, mantle and crust. Gaffey et al. (1993) have discussed this situation at length. These authors suggest that while many asteroids have melts or partial melts on their surfaces, corresponding meteorites are missing. The mineralogy of the CI/CM chondrites appears to be complex intergrowths of fine phases produced by bouts of aqueous alteration and metamorphism, with serpentine as a possible phyllosilicate, which we here identify with C asteroids.

5. Conclusions

We report near-IR spectra for 17 asteroids that belong to the C and X complexes. In order to determine possible surface composition, we collected literature data for these asteroids in the visible and looked for spectral features suggestive of the water and water related components on the asteroids (the UV slope, the 0.7 μm absorption and the 3 μm absorption). Using fairly conservative criteria, we find such evidence in only three of the present 17 asteroids, 34 Circe (0.7 μm feature), 51 Nemausa (UV slope, 0.7 μm, and 3 μm feature), 129 Antigone (3 μm feature), and 191 Kolga (0.7 μm feature). We have assigned classes to these asteroids using literature or on-line facilities and for 14 of the 17 asteroids the spectra are consistent with the properties of the published classes. On the other hand, 191 Kolga has a 0.7 μm feature and while this is not required for its Cb classification according to DeMeo et al. (2009), Vilas (1994) observes that half the C asteroids have this feature.

Of the nine classes represented in the present data, DeMeo et al. (2009) characterize seven by the slopes of their continua in their classification scheme and slope is an important characteristic in the others. In fact, 88% of the variance in C and X asteroid spectra can be explained by continua slope. We thus examined the spectra of the present asteroids in terms of the continuum slopes, plotting the slope between 1.0 and 1.75 μm against the slope between 1.8 and 2.5 μm and call this the continuum plot. We made the break at ~1.8 μm because water features in phyllosilicates (a strong candidate for surface materials on these asteroids) occurs beyond 1.8 μm. Meteorite classes, asteroid classes, terrestrial phyllosilicates, and heated terrestrial phyllosilicates usually plot in discrete and separate fields on these plots, confirming the value of this approach.

On the basis of overlapping in fields on the continuum plots we made associations between asteroid classes and meteorite classes and summarize our suggestions in Table 8. The CI chondrites are linked with the Cgh asteroids, individual CV and CR chondrites

Table 9
Phyllosilicates discussed here with typical terrestrial occurrence.

Terrestrial phyllosilicate	Typical terrestrial occurrence
Kaolinite $Al_2Si_2O_5(OH)_4$	Weathering and decomposition of rocks containing feldspathic minerals (Kruckeberg, 2002; Best, 2003; Evans, 2004).
Serpentine $Mg_3Si_2O_5(OH)_4$	Metamorphic and aqueous alteration of forsterite and pyroxene, replacement other magnesium silicates (Lagasse et al., 2008)
Nontronite, $Na_{0.3}Fe^{+3}{}_2Si_3AlO_{10}(OH)2{\cdot}4(H_2O)$	Weathering of biotite and basalts, precipitation from iron and silicon rich hydrothermal fluids (Bischoff, 1972; Eggleton, 1975).
Montmorillonite (Na, Ca)$_{0.3}$(Al, Mg)$_2Si_4O_{10}(OH)_2(H_2O)_{10}$	Aqueous alteration product of volcanic tuff and ash, pegmatite dikes, wall rocks. Alkaline conditions of poor drainage (Early et al., 1953; Deer et al., 1963; Gaines et al., 1997).
Chlorite $(Mg, Fe^{+2})_5Al(Si_3Al)O_{10}(OH)_8$	Alteration product of mafic minerals such as pyroxenes, amphiboles, and biotite, low-grade metamorphism (Hurlbut and Klein, 1985).

are linked with Xc asteroids, and a CK chondrite is linked with the Ch or Cgh asteroids. A number of unusual CI/CM meteorites are linked with C asteroids, while the CM chondrites are linked with the Xk asteroids. Previous authors have linked the CM chondrites to the Ch asteroids because of the presence of a weak 0.7 μm feature, however their continuum slopes are very different. We argue that continuum slopes are easily and accurately measured, and are sufficiently diagnostic of the various meteorite and asteroid classes to provide important information on asteroid–meteorite linkage.

Most authors agree that the surfaces of the C asteroids are probably in major part phyllosilicates whose spectra are weakened by the presence of opaques and space weathering. We find that the presence of opaques is not alone sufficient to weaken features to the observed degree as stated in Cloutis et al. (1990), and cause the observed continuum slope trends. Neither do we find the grain size variations a likely explanation for the asteroid-to-asteroid spectral differences, although grain size does affect laboratory spectra. Instead, we suggest that the slope difference are the result of asteroid surfaces consisting in large part of the decomposition products of various heated phyllosilicates and in this case can make suggestions as the likely precursor phyllosilicate (and therefore surface composition) on the asteroids. Thus we suggest that for the C complex kaolinite and montmorillonite are possible precursor phyllosilicates, although we rule out kaolinite because it suggests a nonchondritic precursor and has never been observed in chondrites. For the X complex we suggest that precursor phyllosilicates were montmorillonite or serpentines, these minerals have been observed in CM chondrites.

Acknowledgments

We are grateful to Bobby Bus and NASA/NSF for access to the IRTF, Andy Rivkin for help with the correction of spectra for thermal emission, Hazel Sears for reviewing and proofing the manuscript, Beth Clark for very helpful comments, and NASA for grant support. We utilized both the MIT-UH-IRTF Joint Campaign for NEO Reconnaissance and the Bus-DeMeo Taxonomy Classification Web tool and are grateful to the responsible researchers and their funding sources. This research utilizes spectra acquired by Mike Gaffey, Takahiro Hiroi, and Carle Pieters at the NASA RELAB Laboratory at Brown University.

References

Abe, M. et al., 2006. Near-infrared spectral results of Asteroid Itokawa from the Hayabusa spacecraft. Science 312, 1334–1338.
Barber, D.J., Bourdillon, A., Freeman, L.A., 1983. Fe–Ni–S–O layer phase in C2M carbonaceous chondrites – A hydrous sulphide? Nature 305, 295–297.
Bell, J.F., 1988. A probable asteroidal parent body for the CV or CO chondrites. Meteoritics 23, 256–257.
Best, M.G., 2003. Igneous and Metamorphic Petrology, second ed. Blackwell Publishing, Richmond, Victoria, Australia.
Binzel, R.P., Bus, S.J., Burbine, T.H., Sunshine, J.M., 1996. Spectral properties of near-Earth asteroids: Evidence for sources of ordinary chondrite meteorites. Science 273, 946–948.
Binzel, R.P., Rivkin, A.S., Stuart, J.S., Harris, A.W., Bus, S.J., Burbine, T.H., 2004. Observed spectral properties of near-Earth objects: Results for population distribution, source regions, and space weathering processes. Icarus 170, 259–294.
Bischoff, J.L., 1972. A ferroan nontronite from the Red Sea geothermal system. Clays Clay Miner. 20, 217–223.
Brearley, A.J., 2006. The action of water. In: Lauretta, D.S., McSween, H.Y., Jr. (Eds.), Meteorites and the Solar System II. The University of Arizona Press, Tucson, AZ, pp. 584–624.
Britt, D.T., Pieters, C.M., 1994. Darkening in black and gas-rich ordinary chondrites: The spectral effects of opaque morphology and distribution. Geochim. Cosmochim. Acta 58, 3905–3919.
Burbine, T.H., 1998. Could G-class asteroids be the parent bodies of the CM chondrites? Meteor. Planet. Sci. 33, 253–258.
Burbine, T.H., McCoy, T.J., Meibom, A., Gladman, B., Keil, K., 2002. Meteoritic parent bodies: Their number and identification. In: Bottke, W.F., Cellino, A., Paolicchi, P., Binzel, R.P. (Eds.), Asteroids III. The University of Arizona Press, Tucson, AZ, pp. 653–667.
Bus, S.J., Binzel, R.P., 2002. Phase II of the small main-belt asteroid spectroscopic survey: A feature-based taxonomy. Icarus 158, 146–177.
Carvano, J.M., Mothe-Diniz, T., Lazzaro, D., 2003. Search for relations among a sample of 460 asteroids with featureless spectra. Icarus 161, 356–382.
Chamberlin, A.B., Yeomans, D.K., 2010. JPL Small-Body Database Browser. Jet Propulsion Laboratory: Solar System Dynamics. <http://ssd.jpl.nasa.gov/sbdb.cgi#top>.
Chapman, C.R., 1996. S-type asteroids, ordinary chondrites, and space weathering: The evidence from Galileo's fly-bys of Gaspra and Ida. Meteoritics 31, 699–725.
Clark, R.N., 1983. Spectral properties of mixtures of montmorillonite and dark carbon grains: Implications for remote sensing minerals containing chemically and physically adsorbed water. J. Geophys. Res. 88, 10635–10644.
Clark, B.E., Hapke, B., Pieters, C., Britt, D., 2002. Asteroid space weathering and regolith evolution. In: Bottke, W.F., Cellino, A., Paolicchi, P., Binzel, R.P. (Eds.), Asteroids III. The University of Arizona Press, Tucson, AZ, pp. 585–599.
Clark, B.E., et al., 2010. Spectroscopy of B-type asteroids: Subgroups and meteorite analogs. J. Geophys. Res. 115, ID E066005.
Cloutis, E.A., Gaffey, M.J., Smith, D.G.W., Lambert, R.STJ., 1990. Reflectance spectra of mafic silicate-opaque assemblages with applications to meteorite spectra. Icarus 84, 315–333.
Deer, W.A., Howie, R.A., Zussman, J., 1963. Rock-forming minerals. Sheet Silicates, vol. 3. Longmans, London, pp. 226–245.
DeMeo, F.E., Binzel, R.P., Slivan, S.M., Bus, S.J., 2009. An extension of the Bus asteroid taxonomy into the near-infrared. Icarus 202, 160–180.
Descamps, P. et al., 2007. Figure of the double Asteroid 90 Antiope from adaptive optics and lightcurve observations. Icarus 187, 482–499.
Dukes, C.A., Baragiola, R.A., McFadden, L.A., 1999. Surface modification of olivine by H^+ and He^+ bombardment. J. Geophys. Res. 104, 1865–1872.
Early, J.W., Osthaus, B.B., Milne, I.H., 1953. Purification and properties of montmorillonite. Am. Mineral. 38, 707–724.
Eggleton, R.A., 1975. Nontronite topotaxial after hedenbergite. Am. Mineral. 60, 1063–1068.
Evans, B.W., 2004. The serpentinite multisystem revisited: Chrysotile is metastable. Int. Geol. Rev. 46, 479–506.
Feierberg, M.A., Lebofsky, L.A., Tholen, D.J., 1985a. The nature of C-class asteroids from 3-μm spectrophotometry. Icarus 63, 183–191.
Feierberg, M.A., Lebofsky, L.A., Tholen, D.J., 1985b. Are T, P, and D asteroids really ultraprimitive? Bull. Am. Astron. Soc. 17, 730.
Fornasier, S., Lazzarin, M., Barbieri, C., Barucci, M.A., 1999. Spectroscopic comparison of aqueous altered asteroids with CM2 carbonaceous chondrite meteorites. Astron. Astrophys. Suppl. 135, 65–73.
Gaffey, M.J., Burbine, T.H., Binzel, R.P., 1993. Asteroid spectroscopy – Progress and perspectives. Meteoritics 28, 161–187.
Gaffey, M., 2001. Meteorite Spectra. EAR-A-3-RDR-METEORITE-SPECTRA-V2.0. NASA Planetary Data System.
Gaffey, M.J., 2003. Observational and data reduction techniques to optimize mineralogical characterizations of asteroid surface materials. In: 34th Annual Lunar and Planetary Science Conference, March 17–21, 2003, League City, TX, Abstract 1602.
Gaffey, M.j., McCord, T.B., 1978. Asteroid surface material – Mineralogical characterizations from reflectance spectra. Space Sci. Rev. 21, 555–628.
Gaines, R.V., Skinner, H.C.W., Foord, E.E., Mason, B., Rosenweig, A. (Eds.), 1997. Dana's New Mineralogy: The System of Mineralogy of James Dwight Dana and Edward Salisbury Dana, eighth ed. Wiley-Interscience, New York, p. 1483.
Gietzen, K.M., Lacy, C.H.S., Ostrowski, D.R., Sears, D.W.G., submitted for publication. IRTF observations of S complex and other asteroids: Implications for surface compositions, the presence of clinopyroxenes, and their relationship to meteorites. J. Geophys. Res. – Planets.
Hiroi, T., Pieters, C.M., Zolensky, M.E., Lipschutz, M.E., 1993. Evidence of thermal metamorphism on the C, G, B, and F asteroids. Science 261, 1016–1018.
Hiroi, T., Zolensky, M.E., Pieters, C.M., Lipschutz, M.E., 1996. Thermal metamorphism of the C, G, B, and F asteroids seen from the 0.7 μm, 3 μm, and UV absorption strengths in comparison with carbonaceous chondrites. Meteor. Planet. Sci. 31, 321–327.
Hiroi, T., Zolensky, M.E., 1999. UV–VIS–NIR absorption features of heated phyllosilicates as remote-sensing clues of thermal histories of primitive asteroids. Antarctic Meteor. Res. 12, 108–116.
Hurlbut, C.S., Klein, C., 1985. Manual of Mineralogy, 20th ed. John Wiley and Sons, New York.
Jarosewich, E., 1990. Chemical analyses of meteorites: A compilation of stony and iron meteorite analyses. Meteoritics 25, 323–337.
Jones, T.D., Lebofsky, L.A., Lewis, J.S., Marley, M.S., 1990. The composition and origin of the C, P, and D asteroids: Water as a tracer of thermal evolution in the outer belt. Icarus 88, 172–192.
Keil, K., 1982. Composition and origin of chondritic breccias. In: Taylor, G.J., Wilkening, L.L. (Eds.), Workshop on Lunar Breccias and Soil and their Meteoritic Analogs, LPI Tech. Rpt. 82-02, Lunar and Planetary Institute, Houston, pp. 65–83.
Keller, L.P., Wentworth, S.J., McKay, D.S., Taylor, L.A., Pieters, C., Morris, R.V., 1999. Space Weathering in the Fine Size Fractions of Lunar Soils: Soil Maturity Effects Workshop on New Views of the Moon II: Understanding the Moon through the Integration of Diverse Datasets, September 22–24, 1999, Flagstaff, AZ, Abstract 8052.
Kristensen, L.K., 1991. The rotation of (51) Nemausa. Astron. Nach. 312, 209–220.
Kruckeberg, A.R., 2002. Geology and Plant Life: The Effects of Landforms and Rock Types on Planets. University of Washington Press, Seattle.
Lagasse, P., Goldman, L., Hobson, A., Norton, S.R. (Eds.), 2008. The Columbia Encyclopedia, sixth ed. Columbia University Press, New York.

Lazzarin, M., Marchi, S., Magrin, S., Barbieri, C., 2004. Visible spectral properties of Asteroid 21 Lutetia, target of Rosetta Mission. Astron. Astrophys. 425, L25–L28.
Lebofsky, L.A., 1978. Asteroid 1 Ceres – Evidence for water of hydration. Mon. Not. R. Astron. Soc. 182, 17P–21P.
Lebofsky, L.A., 1980. Infrared reflectance spectra of asteroids: A search for water of hydration. Astron. J. 85, 573–585.
Mackinnon, I.D.R., Zolensky, M.E., 1984. Proposed structures for poorly characterized phases in C2M carbonaceous chondrite meteorites. Nature 309, 240–242.
McFadden, L.A., Wellnitz, D.D., Schnaubelt, M., Gaffey, M.J., Bell, J.F., Izenberg, N., Murchie, S., Chapman, C.R., 2001. Mineralogical interpretation of reflectance spectra of Eros from NEAR near-infrared spectrometer low phase flyby. Meteor. Planet. Sci. 36, 1711–1726.
McKay, D.S., Heiken, G., Basu, A., Blanford, G., Simon, S., Reedy, R., French, B.M., Papike, J., 1991. The lunar regolith. In: Heiken, G.H., Vaniman, D.T., French, B.M. (Eds.), Lunar Sourcebook: A User's Guide to the Moon. Cambridge University Press, pp. 285–356.
McSween, H.Y., Richardson Jr., S.M., 1977. The composition of carbonaceous chondrite matrix. Geochim. Cosmochim. Acta 41, 1145–1161.
Milliken, R.E., Mustard, J.F., 2007. Estimating the water content of hydrated minerals using reflectance spectroscopy. I: Effects of darkening agents and low-albedo materials. Icarus 189, 550–573.
Nichols Jr., R.H., Hohenberg, C.M., Olinger, C.T., 1994. Implanted solar helium, neon, and argon in individual lunar ilmenite grains – Surface effects and a temporal variation in the solar wind composition. Geochim. Cosmochim. Acta 58, 1031–1042.
Nolan, M.C. et al., 2008. (153591) 2001 SN_263. Central Bureau Electronic Telegrams 1254, 1.
Ohtsuka, K., Sekiguchi, T., Kinoshita, D., Watanabe, J.-I., Ito, T., Arakida, H., Kasuga, T., 2006. Apollo Asteroid 2005 UD: Split nucleus of (3200) Phaethon? Astron. Astrophys. 450, L25–L28.
Ostrowski, D.R., Sears, D.W.G., Gietzen, K.M., Lacy, C.H.S., 2008a. Spectral features in C and C-like asteroids and the possible presence of phyllosilicates. In: 39th Lunar Planet Science Conference, League City, TX, March 10–14, 2008. LPI Contribution No. 1391. Abstract #1061.
Ostrowski, D.R., Sears, D.W.G., Gietzen, K.M., Lacy, C.H.S., 2008b. A study of phyllosilicates as possible components of the surface of C asteroids. In: Asteroids, Comets, Meteors 2008, Baltimore, MD, July 14–18, 2008. LPI Contribution No. 1405, Abstract #8299.
Ostrowski, D.R., Sears, D.W.G., Lacy, C.H.S., Gietzen, K.M., 2009a. Asteroidal origins for carbonaceous chondrites. Meteor. Planet. Sci. Suppl., Abstract #5309.
Ostrowski, D.R., Sears, D.W.G., Gietzen, K.M., Lacy, C.H.S., 2009b. An investigation of phyllosilicates, C chondrites, and C asteroids using continuum slopes of near infrared spectra. Lunar Planet. Sci. 40, Abstract #1136.
Ostrowski, D.R., Gietzen, K., Lacy, C., Sears, D.W.G., 2010. An investigation of the presence and nature of phyllosilicates on the surface of C asteroids by an analysis of the continuum slopes in their near infrared spectra. Meteor. Planet. Sci. 45, 615–637.
Pieters, C.M., Taylor, L.A., Noble, S.K., Keller, L.P., Hapke, B., Morris, R.V., Allen, C.C., McKay, D.S., Wentworth, S., 2000. Space weathering on airless bodies: Resolving a mystery with lunar samples. Meteor. Planet. Sci. 35, 1101–1107.
Polishook, D., Brosch, N., 2008. Photometry of Aten asteroids – More than a handful of binaries. Icarus 194, 111–124.
Pravec, P. et al., 2005. Tumbling asteroids. Icarus 173, 108–131.
Rayner, J.T., Toomey, D.W., Onaka, P.M., Denault, A.J., Stahlberger, W.E., Vacca, W.D., Cushing, M.C., Wang, S., 2003. SpeX: A medium-resolution 0.8–5.5 micron spectrograph and imager for the NASA infrared telescope facility. Publ. Astron. Soc. Pacific 115, 362–382.
Rivkin, A.S., 1997. Observation of main-belt asteroids in the 3-MICRON region. Ph.D. Thesis, University of Arizona.
Rivkin, A.S., Neese, C., 2003. Rivkin three micron asteroid data. EAR-A-3-RDR-RIVKIN-THREE-MICRON-V3.0. NASA Planetary Data System.
Rivkin, A.S., Howell, E.S., Vilas, F., Lebofsky, L.A., 2002. Hydrated minerals on asteroids: The astronomical record. In: Bottke, W.F., Jr., Cellino, A., Paolicchi, P., Binzel, R.P. (Eds.), Asteroids III. University of Arizona Press, Tucson, pp. 235–253.
Rivkin, A.S., Binzel, R.P., Bus, S.J., 2005. Constraining near-Earth object albedos using near-infrared spectroscopy. Icarus 175, 175–180.
Rivkin, A.S., Volquardsen, E.L., Clark, B.E., 2006. The surface composition of Ceres: Discovery of carbonates and iron-rich clays. Icarus 185, 563–567.
Rubin, A.E., 1997. Mineralogy of meteorite groups. Meteor. Planet. Sci. 32, 231–247.
Sasaki, S., Hiroi, T., Nakamura, K., Hamabe, Y., Kurahashi, E., Yamada, M., 2002. Simulation of space weathering by nanosecond pulse laser heating: Dependence on mineral composition, weathering trend of asteroids and discovery of nanophase iron particles. Adv. Space Res. 29, 783–788.
Sawyer, S.R., 1991. A high-resolution CCD spectroscopic survey of low-albedo main belt asteroids. Ph.D. Thesis, The University of Texas at Austin.
Sears, D. et al., 2004. The Hera mission: Multiple near-Earth asteroid sample return. Adv. Space Res. 34, 2270–2275.
Sears, D.W.G., Gietzen, K., Ostrowski, D., Lacy, C., Chevrier, V., 2008a. Primitive materials on asteroids. Meteor. Planet. Sci. Suppl. A43, Abstract #5237.
Sears, Derek W.G., Gietzen, K., Ostrowski, D., Lacy, C., Chevrier, V., 2008b. Primitive materials on asteroids. American Astronomical Society, DPS meeting #40, #60.05. Bulletin of the American Astronomical Society, vol. 40, p. 508.
Sullivan, R.J., Thomas, P.C., Murchie, S.L., Robinson, M.S., 2002. Asteroid geology from Galileo and NEAR Shoemaker data. In: Bottke, W.F., Jr., Cellino, A., Paolicchi, P., Binzel, R.P. (Eds.), Asteroids III. University of Arizona Press, Tucson, pp. 331–350.
Sunshine, J.M., Pieters, C.M., 1993. Estimating modal abundances from the spectra of natural and laboratory pyroxene mixtures using the modified Gaussian model. J. Geophys. Res. 98, 9075–9087.
Tholen, D.J., 1989. Asteroid taxonomic classifications. In: Binzel, R.P., Gehrels, T., Matthews, M.S. (Eds.), Asteroids II. University of Arizona Press, Tucson, pp. 1139–1150.
Tomeoka, K., Buseck, P.R., 1985. Indicators of aqueous alteration in CM carbonaceous chondrites: Microtextures of a layered mineral containing Fe, S, O and Ni. Geochim. Cosmochim. Acta 49, 2149–2163.
Vacca, W.D., Cushing, M.C., Rayner, J.T., 2003. A method of correcting near-infrared spectra for telluric absorption. Publ. Astron. Soc. Pacific 115, 389–409.
Vilas, F., 1994. A cheaper, faster, better way to detect water of hydration on Solar System bodies. Icarus 111, 456–467.
Vilas, F., Gaffey, M.J., 1989. Phyllosilicate absorption features in main-belt and outer-belt asteroids reflectance spectra. Science 246, 790–792.
Vilas, F., Hiroi, T., Zolensky, M.E., 1993. Comparison of visible and near-infrared reflectance spectra of CM2 carbonaceous chondrites and primitive asteroids. Lunar Planet. Sci. 24, Part 3: N-Z, Lunar and Planetary Institute, pp. 1465–1466.
Wiik, H.B., 1969. On regular discontinuities in the composition of meteorites. Comment. Phys. Math. 34, 135–145.
Xu, S., Binzel, R.P., Burbine, T.H., Bus, S.J., 1995. Small main-belt asteroid spectroscopic survey: Initial results. Icarus 115, 1–35.
Zellner, B., Leake, M., Lebertre, T., Duseaux, M., Dollfus, A., 1977. The asteroid albedo scale. I. Laboratory polarimetry of meteorites. Proc. Lunar Sci. Conf. 8, vol. 1, Houston, TX, March 14–18, 1977. Pergamon Press, Inc., New York (A78-41551 18-91), pp. 1091–1110.
Zellner, B., Tholen, D.J., Tedesco, E.F., 1985. The eight-color asteroid survey: Results for 589 minor planets. Icarus 61, 335–416.